A constitutive model for fault gouge deformation in dynamic rupture simulations

Eric G. Daub and Jean M. Carlson

Department of Physics, University of California, Santa Barbara, California, USA

Abstract. In the context of numerical simulations of elastodynamic ruptures, we compare friction laws, including the linear slip-weakening (SW) law, the Dieterich-Ruina (DR) law, and the Free Volume (FV) law. The FV law is based on microscopic physics, incorporating Shear Transformation Zone (STZ) Theory which describes local, non-affine rearrangements within the granular fault gouge. A dynamic state variable models dilation and compaction of the gouge, and accounts for weakening and re-strengthening in the FV law. The principal difference between the FV law and the DR law is associated with the characteristic length scale L. In the FV law, L_{FV} grows with increasing slip rate, while in the DR law L_{DR} is independent of slip rate. The length scale for friction is observed to vary with slip velocity in laboratory experiments with simulated fault gouge, suggesting that the FV law captures an essential feature of gouge-filled faults. In simulations of spontaneous elastodynamic rupture, for equal energy dissipation the FV law produces ruptures with smaller nucleation lengths, lower peak slip velocities, and increased slip required for friction to fully weaken to steady sliding when compared to ruptures governed by the SW or DR laws. We also examine generalizations of the DR and FV laws that incorporate rapid velocity weakening. The rapid weakening laws produce self-healing slip pulse ruptures for low initial shear loads. For parameters which produce identical net slip in the pulses of each rapid weakening friction law, the FV law exhibits a much shorter nucleation length, a larger slip-weakening distance, and less frictional energy dissipation than corresponding ruptures obtained using the DR law.

1. Introduction

In simulations of dynamic earthquake rupture, friction laws link characteristics of microscopic adhesion and dissipation to their implications for fault-scale behavior. A variety of friction laws have been studied in the context of individual ruptures [e.g., *Perrin et al.*, 1995; *Zheng and Rice*, 1998; *Nielsen et al.*, 2000; *Nielsen and Carlson*, 2000; *Bizzarri and Cocco*, 2005] and sequences of earthquakes [e.g, *Carlson and Langer*, 1989; *Cochard and Madariaga*, 1996; *Shaw and Rice*, 2000]. Determining how friction laws arise from microscopic mechanisms and lead to complex behavior remains a central question in earthquake source physics.

Constitutive laws governing dynamic rupture models can be divided into two classes: (1) single variable slip-dependent or velocity-dependent laws, where shear stress weakens according to an *a priori* fixed function of slip or slip velocity, and (2) rate and state laws, which incorporate explicit rate (i.e. velocity) dependence and one or more physically motivated thermodynamic-like state variables to capture the history dependence of friction. In the single variable category, we consider the linear slip-weakening (SW) law [*Ida*, 1972; *Andrews*, 1976a,b], which is the most widely studied example in this class in the geophysical literature. The rate and state laws that we study include the Dieterich-Ruina (DR) law [*Dieterich*, 1979; *Ruina*, 1980] and the Free Volume (FV) law, which connects fault evolution to microscopic physical processes in a layer of fault gouge [*Lemaitre*, 2002].

The linear SW law is frequently used as a simplified description of friction. The law prescribes a specific linear relationship between slip and weakening of the shear stress, depends on few parameters, and ignores more complicated processes such as dynamic re-strengthening and slip rate dependence. The DR law adds experimentally observed slip rate dependence, and re-establishes frictional strength after weakening through state variable evolution. The FV law uses Shear Transformation Zone Theory [*Falk and Langer*, 1998, 2000] to model the plastic deformation of granular fault gouge, and incorporates dilation and compaction as the basis for fault weakening and re-strengthening, respectively. An alternative interpretation of the weakening and strengthening processes is given in terms of an effective temperature (a measure of local disorder) [*Langer*, 2008], which will be discussed in Section 5.

The FV law provides a good description of laboratory experiments for boundary lubrication [*Lemaitre and Carlson*, 2004] and numerical simulations of dense granular flows [*Lois et al.*, 2005]. In this study, we extend these investigations to fault-scale behavior and compare the FV law to the SW and DR law, contrasting their implications for dynamic rupture. Additionally, we consider versions of the DR and FV laws modified to include rapid velocity weakening. Because the physics of the earthquake source is poorly constrained, examining the dynamic ruptures that arise from different friction laws can aid seismologists in assessing the range of possible physical outcomes occurring at the earthquake source.

2. Constitutive Models

In this section we describe the first three friction laws used in our analysis of dynamic rupture. The linear SW law and the DR law have already been discussed extensively in the literature; our comments on those are brief. We summarize the physics of the FV law and and present the equations in this section. The FV law has not been studied in the

0148-0227/09/$9.00

context of earthquake simulations, and because of this we include a complete discussion of its derivation in the Appendix A. Rapid weakening laws are discussed in Section 4.

2.1. Linear Slip-Weakening

Linear slip-weakening [*Ida*, 1972; *Andrews*, 1976a,b] has been used extensively to study dynamic rupture [e.g., *Andrews*, 1976a,b; *Day*, 1982; *Harris and Day*, 1993; *Madariaga et al.*, 1998]. Shear stress τ is a linearly decreasing function of slip u up to some slip-weakening distance d_c, beyond which a constant stress is prescribed:

$$\tau = \begin{cases} \tau_p - (\tau_p - \tau_d)\,\frac{u}{d_c}, & (u \le d_c); \\ \tau_d, & (u > d_c). \end{cases} \tag{1}$$

The fault is initially locked. Shear stress increases to the yield stress τ_p before initiating slip, and then weakens as the fault slips (Fig. 1). Stress is a fixed function of slip, which sets the amount of energy lost to fracture and frictional dissipation (the area under the curve plotting shear stress as a function of slip). Because the stress τ_d is constant, the fault cannot regain strength once it ruptures. The SW law is intentionally simple, and serves as a first approximation for how stress weakens with slip. However, laboratory experiments show that there is explicit velocity dependence of friction, as well as time dependent re-strengthening [*Dieterich*, 1972]. This laboratory work led to the development of the DR law.

2.2. Dieterich-Ruina Law

The DR law is a phenomenological friction law, introduced to capture experimental observations of both steady state and transient friction [*Dieterich*, 1979]. The DR law is a rate and state friction law that assumes dependence on a single dynamic state variable. Shear stress τ is a function of rate (slip velocity V) and the state variable θ. The dependence on both rate and state is logarithmic in the DR law:

$$\tau = \sigma \left[f_0 + a \log\left(\frac{V}{V_0}\right) + b \log\left(\frac{\theta V_0}{l}\right)\right]. \tag{2}$$

Other parameters in the law are normal stress σ, constants a and b determining the rate and state dependence, length scale l, and reference friction coefficient and slip velocity, f_0 and V_0, respectively. In this study, we use the ageing law for state evolution [*Ruina*, 1983],

$$\frac{d\theta}{dt} = 1 - \frac{\theta V}{l}. \tag{3}$$

The state variable θ has dimensions of time and is often interpreted as the lifetime of surface asperity contacts, confirmed experimentally by *Dieterich and Kilgore* [1994]. A common alternative to this state variable evolution law is the slip law [*Ruina*, 1983]. However, because the ageing law is more frequently used in earthquake modeling and includes time-depedent healing, which is also present in the Free Volume law, we focus on the ageing law in this study.

At a constant slip velocity V_{ss}, the state variable has a steady-state solution $\theta_{ss} = l/V_{ss}$ and the shear stress is

$$\tau_{ss} = \sigma \left[f_0 + (a-b) \log\left(\frac{V_{ss}}{V_0}\right)\right]. \tag{4}$$

The relative values of a and b determine the sign of the velocity dependence. Stick-slip instabilities arise only in friction laws with steady-state velocity weakening [*Rice and Ruina*, 1983], so we take $b > a$.

The transient behavior of the DR law is illustrated by a velocity step experiment. A single degree of freedom block is driven by an externally imposed velocity. Alternatively, one can interpret the velocity step as the response of a single degree of freedom elastic slider in the limit of an infinitely stiff spring constant. The block initially slides at the steady-state velocity V_{ss} with the state variable at the corresponding steady-state value, $\theta_{ss} = l/V_{ss}$. This is followed by a sudden step increase ΔV in the imposed sliding velocity. The dynamic response of the slider is shown in Fig. 2. Initially, shear stress increases (the so-called "Direct Effect"); the magnitude of the increase is defined to be A. Over some characteristic length scale, defined to be L, the frictional stress evolves to its new value. The difference between the initial steady-state value of the stress and the new steady-state is defined to be $A - B$ (the "Evolution Effect" is quantified by B). Mathematically, these parameters are identified by [*Rice*, 1983; *Zheng and Rice*, 1998]

$$A = V \frac{\partial \tau}{\partial V}\bigg|_{V=V_{ss},\theta=\theta_{ss}}; \tag{5}$$

$$A - B = V \frac{d\tau_{ss}}{dV}\bigg|_{V=V_{ss}}; \tag{6}$$

$$L = -\frac{V}{\frac{\partial (d\theta/dt)}{\partial \theta}}\bigg|_{V=V_{ss},\theta=\theta_{ss}}. \tag{7}$$

The quantities A and L are evaluated at the initial steady-state values of the velocity and state variable, and $A-B$ at the initial steady state velocity. The quantities A, $A-B$, and L can be calculated for any rate and state law, and laws with more than one state variable will have a length scale associated with each state variable. We attach a subscript when referring to these quantities calculated for a specific friction law to distinguish them from the general definitions. For the DR law, applying Eq. (5)-(7) to Eq. (2) and (3) results in the following:

$$A_{\mathrm{DR}} = \sigma a; \tag{8}$$

$$(A-B)_{\mathrm{DR}} = \sigma\,(a-b)\,; \tag{9}$$

$$L_{\mathrm{DR}} = l. \tag{10}$$

This demonstrates that a and b determine the velocity dependence of friction, and that there is a fixed length scale l for transient effects.

The logarithmic form of Eq. (2) poses a problem at $V = 0$. Several methods of regularization have been used. We follow the common practice of imposing a cutoff velocity V_1 at low slip rates [*Perrin et al.*, 1995; *Zheng and Rice*, 1998; *Favreau et al.*, 1999], and V is replaced by $V + V_1$ in Eqs. (2) and (3). This regularization allows the fault to lock, and the static friction τ_s is defined by an inequality:

$$\tau_s \le \sigma \left[f_0 + a \log\left(\frac{V_1}{V_0}\right) + b \log\left(\frac{\theta V_0}{l}\right)\right]. \tag{11}$$

We use the regularized form of the DR law in our dynamic rupture models. While such a regularization is not required [*Bizzarri et al.*, 2001], adding a cutoff velocity does not significantly affect the friction law at the slip rates of dynamic rupture and ensures that the DR law gives sensible values for the shear stress when $V = 0$.

2.3. Free Volume Law

The Free Volume law is based on Shear Transformation Zone (STZ) Theory, a continuum approximation for amorphous materials such as granular fault gouge. Simulations show that when an amorphous material is sheared, inelastic deformation occurs in localized regions, which switch between two possible orientations [*Falk and Langer*, 1998,

2000]. One such event is illustrated in Fig. 3. These regions are referred to as STZs, and switching orientations generates a fixed amount of inelastic strain and requires a minimum shear stress to switch. STZs are observed to flip only once in simulations, but additional shear creates and destroys STZs to sustain the plastic flow. We assume that the STZs are uniformly distributed throughout the gouge layer. STZs will involve small groups of particles, so the scale of an STZ is much smaller than the total thickness of the slipping zone due to the finely granulated nature of fault cores (or Principal Slip Zones) [*Chester and Chester*, 1998].

The details of STZ reversals depend on two quantites, the applied shear stress and the free volume χ. The free volume is a dimensionless, intensive quantity that describes the density of the fault gouge. It is related to porosity, which is also dimensionless, intensive, and describes the gouge density. They differ because $\chi = 0$ corresponds to the gouge arranged to have the smallest possible volume, also known as random close packing [*Scott and Kilgour*, 1969], which still has some pore space. Free volume is related to porosity ϕ by $\chi = \phi - \phi_0$, so that when $\chi = 0$ the porosity is equal to ϕ_0, the porosity of the random close packing. Smaller values of the free volume correspond to larger density, and as the free volume increases STZs reverse more readily. Increasing the shear stress also increases the frequency at which STZs reverse. The total slip rate on the fault is the combination of these two contributions:

$$V = R\left(\tau\right) \exp\left[-\left(\chi_s + \chi_h\right)/\chi\right] \tag{12}$$

The function $R(\tau)$ describes how frequently the STZs reverse due to the applied stress. We choose an exponential function for $R(\tau)$, which is based on an Eyring model [*Eyring*, 1936] and gives logarithmic velocity dependence in steady-state. The free volume dependence assumes that voids in the gouge are Poisson distributed.

Free volume evolves dynamically as the gouge is sheared. We include terms for compaction, which is time-dependent, and dilation, which occurs at a rate proportional to the rate at which frictional energy is dissipated:

$$\frac{d\chi}{dt} = -R_c \exp\left(-\chi_c/\chi\right) + \alpha\tau V. \tag{13}$$

The evolution of the free volume accounts for the history dependence of friction in the FV law. This dynamic equation can be converted to a porosity evolution equation (using $\chi = \phi - \phi_0$), and is an alternative to the porosity evolution proposed in *Segall and Rice* [1995].

The full equations of the FV law are:

$$\begin{aligned} V &= V_* \exp\left[-f_* - \left(\chi_s + \chi_h\right)/\chi\right]\left(1 - m_0\right) \\ &\quad \times \sinh\left(\tau/\sigma_d\right); \end{aligned} \tag{14}$$

$$\frac{d\chi}{dt} = -R_c \exp\left(-\chi_c/\chi\right) + \alpha\tau V. \tag{15}$$

The FV law allows for solutions that are jammed ($V = 0$) and slipping ($V > 0$). The two different solutions are incorporated using the variable m_0. The values that m_0 takes depend on whether the stress is above or below the minimum stress needed to flip an STZ, $\tau_0 \exp(\chi_h/\chi)$:

$$m_0 = \begin{cases} 1, & [\tau \le \tau_0 \exp\left(\chi_h/\chi\right)]; \\ \frac{\tau_0}{\tau} \exp\left(\chi_h/\chi\right), & [\tau > \tau_0 \exp\left(\chi_h/\chi\right)]. \end{cases} \tag{16}$$

The parameters in the FV law include the characteristic slip rate V_*, the STZ activation energy scaled by the thermal energy f_*, the characteristic free volume for shearing χ_s, the characteristic free volume for STZ creation χ_h, the STZ activation stress σ_d, the compaction rate R_c, the characteristic free volume for compaction χ_c, the fraction of frictional energy that goes into dilating the fault gouge α, and the STZ yield stress τ_0. The three characteristic free volumes are distinct quantities, as each corresponds to a different rearrangement of the fault gouge. We also note that the STZ activation stress σ_d, also known as the direct effect stress in rock mechanics experiments, determines the instantaneous stress change due to a change in the slip rate. This stress is typically much smaller than the normal stress or the shear stress in laboratory experiments.

Calculation of quantities A, $A - B$, and L (Eq. (5)-(7)) for the FV law enables a direct comparison with the equivalent parameters for the DR law. The resulting equations are rather cumbersome (see Appendix B). Approximate expressions for A_{FV}, $(A - B)_{\mathrm{FV}}$, and L_{FV} are:

$$A_{\mathrm{FV}} \approx \sigma_d; \tag{17}$$

$$(A - B)_{\mathrm{FV}} \approx \sigma_d\left[1 - \left(\chi_s + \chi_h\right)/\chi_c\right]; \tag{18}$$

$$L_{\mathrm{FV}} \approx \frac{\chi_{ss}^2}{\alpha\chi_c\tau_{ss}} = \frac{\chi_c}{\alpha\tau_{ss}\left[\log\left(\frac{R_c}{\alpha\tau_{ss}V_{ss}}\right)\right]^2}. \tag{19}$$

The steady-state value of the shear stress τ_{ss} is found by simultaneously solving Eq. (14) (with the stress, free volume, and slip rate at steady-state) and the steady-state expression for the free volume $\chi_{ss} = \chi_c/\log(R_c/(\alpha\tau_{ss}V_{ss}))$. Note that τ_{ss} depends on the slip rate, though it turns out that the stress does not change as much as the free volume with varying slip rates due to the logarithmic velocity dependence. These approximations assume that $\sigma_d/\tau_{ss} << 1$ (i.e. the typical shear stress is much larger than the transient stress increase needed to flip an STZ) and that the stress is not close to the yield stress. The approximate values (Eq. (17)-(19)) are within a few percent of the exact values for the parameters we choose as long as the steady-state stress is not near the yield stress (deviations from Eq. (17)-(19) are most significant if $m_0 \approx 1$). The approximation that the stress is not near the yield stress is appropriate for analysis of velocity step experiments where the slip rate is perturbed from steady sliding and the fault never stops sliding. However, when studying dynamic rupture, slip often initiates on a locked fault and deviations from these expressions can be more significant. Therefore, these expressions are useful in comparing the law to laboratory experiments, while the exact constitutive law (Eq. (14)-(15)) is implemented into the dynamic rupture calulations. In our rupture simulations, we always start the fault at $V = 0$ for simplicity, but rapid slip acceleration can still occur if the fault begins with a slip rate much slower than seismic slip rates.

The quantities A_{FV} and $(A-B)_{\mathrm{FV}}$ are independent of slip rate, as are the corresponding values in the DR law A_{DR} and $(A - B)_{\mathrm{DR}}$. This verifies that the STZ activation stress σ_d is equivalent to the DR law direct effect stress $a\sigma$. Since the direct effect in the DR law is proportional to the effective normal stress, σ_d should also be proportional to the effective normal stress with a similar proportionality constant. The steady-state velocity dependence of both laws is logarithmic. If the reference free volumes satisfy $\chi_s + \chi_h > \chi_c$, the free volume law is steady-state velocity weakening. In this manner, the FV law allows for the physical interpretation that the velocity dependence of friction is based on the relative values of these three characteristic free volumes. In the steady-state velocity weakening regime, as the slip velocity increases, the rate at which STZs flip orientation grows faster than the rate at which the gouge compacts. Therefore, lower stress is required to balance compaction and dilation to maintain the steady-state value of the free volume. The FV law predicts dilatancy hardening and steady-state velocity strengthening if $\chi_s + \chi_h < \chi_c$. Parameters in this regime do not allow for earthquake instabilities.

In experiments on laboratory faults, velocity weakening is usually not observed until strain localizes to a narrow shear band. Since the FV law assumes uniform strain througout the gouge, we focus on matching the behavior of laboratory experiments once they reach the velocity weakening regime and a narrower active shearing thickness is established. One way to reconcile the observed trend in the velocity dependence of experiments with the velocity dependence of the FV law is to note that the reference free volumes depend on the constitutients of the gouge. Since wear and comminution occur throughout the experiments, the reference free volumes could change (for instance, creation of smaller grains could decrease χ_c) to match the observed trend towards velocity weakening. These changes modify the porosity ϕ without significantly changing the shearing thickness w. Since such changes alter the free volume and the reference free volumes, this will significantly alter the frictional properties of the gouge.

Figure 4 shows a plot of shear stress and free volume/porosity as a function of shear displacement for two different velocity steps. This verifies that $A_{\rm FV}$ and $(A-B)_{\rm FV}$ are independent of slip rate. The transient changes in stress are the same regardless of the sliding velocity, which confirms the predictions of Eq. (17)-(18).

The key difference between the two friction laws involves the length scale for state variable evolution L. The length scale in the DR law $L_{\rm DR}$ is constant, while the length scale for the FV law $L_{\rm FV}$ varies with slip velocity (Eq. (19)). In the FV law, in order to slip steadily at a higher velocity, the material must dilate (though the plot in Fig. 4 shows that the changes in porosity are small compared to the overall porosity, so the layer thickness does not change significantly). Our calculation shows that $L_{\rm FV}$ is proportional to the square of the steady-state free volume and increases at higher slip rates. In the DR law, the natural length scale is the size of asperity contacts, which is independent of the slip rate and exhibits no velocity dependence. Seismic slip velocities range over many orders of magnitude, from slow quasistatic loading to unstable rapid slip. The varying length scale in the FV law has a potentially large impact.

Mair and Marone [1999] observe systematic variations of the slip distance with slip rate for friction evolution in experiments involving fault gouge. Figure 5 compares the FV law and their laboratory data. Values of $L_{\rm FV}$ are calculated from Eq. (19). We note variations in $L_{\rm FV}$ with slip velocity that exhibit behavior very similar to laboratory faults. This suggests the FV law may capture important behavior for gouge filled faults which is absent in the DR law.

The plots in Fig. 4 show that the length scale $L_{\rm FV}$ depends on the slip rate. The displacement needed for stress to weaken to its new steady value is larger in the second velocity step (from 10^{-5} m/s to 10^{-4} m/s) than in the first velocity step (from 10^{-6} m/s to 10^{-5} m/s). This is easiest to see in the lower plot in Fig. 4, as the free volume is still evolving at the right edge of the plot while the free volume has stabilized within the same displacement during the previous velocity step.

In addition to the slip rate dependence of $L_{\rm FV}$, the FV law provides a means to quantitatively bridge the difference in scales between laboratory faults and natural faults. Because the DR law is phenomenological, it is difficult to estimate precisely how the DR parameters a, b, and l (Eq. 2) may or may not depend on the scale of the fault. The FV law based on grain-scale physics includes a specification for how parameters depend on the scale of the fault or experiment. The dilation coefficient α is inversely proportional to the slipping thickness w. This is because the dilation term depends on the strain rate. The strain rate will be larger for a thinner layer at a given slip velocity, and the scaling of α with w reflects this. The FV Law predicts $L_{\rm FV} \propto w$ (since $L_{\rm FV} \propto 1/\alpha$ and $\alpha \propto 1/w$), and increasing the width of the gouge layer increases the length scale in the FV law. This predicted scaling is consistent with the experiments of *Marone and Kilgore* [1993]. This suggests natural faults exhibit a length scale a few orders of magnitude greater than laboratory values. The direct effect $A_{\rm FV}$ and the steady-state velocity dependence $(A-B)_{\rm FV}$ are independent of the layer thickness w, and remain unchanged with fault scale.

The thickness of the actively shearing layer in laboratory experiments cannot be directly measured since strain tends to localize within the gouge during experiments. Because strain localizes over many velocity steps, we assume that during an individual veloctiy step the shear band thickness is uniform, and the uniform shear assumption in the FV law is a good approximation for that single velocity step. We can then use the FV law to estimate the shear band thickness of the laboratory experiments. Using the same parameters as in Fig. 5, we can calculate the change in free volume due to a velocity step. The change in pore space is due to layer dilation, so the additional porosity due to dilation is approximately dw/w, where dw is the measured change in layer thickness. Therefore, the change in free volume $d\chi$ (equal to the porosity change) is related to the layer thickness w and the thickness change dw by $d\chi = dw/w$, so given an experimental value of dw an estimate of w can be computed. We find that with $w = 0.75$ mm, the FV law follows the dilation data for experiments in the velocity weakening regime [*Mair and Marone*, 1999]. This calculated value is also within reason given the microstructural observations in the experiments. For natural faults we estimate $w = 0.45$ m, a typical thickness of the gouge layer in a study by *Chester and Chester* [1998]. The estimates of w for laboratory and natural faults allow us to determine the parameters for our rupture dynamics simulations for natural faults.

3. Dynamic Ruptures

In this section, we compare the effects of the SW, DR, and FV laws in the spontaneous propagation of elastodynamic ruptures. The previous section considers small single degree of freedom sliders to determine A, $A-B$, and L for each law. Now we numerically simulate ruptures that propagate along faults for which the length is typically orders of magnitude larger than laboratory samples. Comparisons between the SW and DR laws have been made for dynamic rupture simulations [*Bizzarri et al.*, 2001]. Here we extend comparisons to include the FV law.

We model the fault as the interface between two homogeneous, isotropic, linear elastic half spaces (Fig. 6). The fault is the xy plane, and this boundary is governed by the chosen friction law. We consider only simple 2D in-plane or anti-plane ruptures, and thus by symmetry all quantities on the fault plane have no y dependence. Due to this imposed in-plane or anti-plane geometry, the vector slip velocity reduces to a scalar $V(x,t)$, and the stress tensor has only one shear component $\tau(x,t)$. For in-plane ruptures, the slip velocity only has a component in the x-direction ($V(x,t) = V_x(x,t)$) and the shear stress is the xz-component ($\tau(x,t) = \tau_{xz}(x,t)$), while in anti-plane problems the slip rate has only a y-component ($V(x,t) = V_y(x,t)$) and the shear stress is the yz-component ($\tau(x,t) = \tau_{yz}(x,t)$).

The elastodynamic equation requires that on the fault plane, the shear stress $\tau(x,t)$ and the slip velocity $V(x,t)$ satisfy [*Cochard and Madariaga*, 1994; *Perrin et al.*, 1995]

$$\tau(x,t) = \tau_{\rm load}(x) + f(x,t) - \frac{\mu}{2c_s} V(x,t). \qquad (20)$$

The stress and slip rate also satisfy the friction law on the fault, and the two equations are solved simultaneously. The initial loading stress $\tau_{\rm load}(x)$ is constant except for a small

overstressed patch spanning the full depth of the fault of width $L_{\rm trig}$ (where the initial load is $\tau_{\rm trigg}$). This patch, the medium shade of gray in Fig. 6, nucleates the rupture. This does not capture the slow nucleation process that initiates real earthquakes, but this simple nucleation procedure preserves the differences between ruptures with various friction laws. The stress transfer functional $f(x,t)$ tracks dynamic stress changes due to past fault slip, and the final term explicitly extracts radiation damping [*Cochard and Madariaga*, 1994], where c_s is the shear wave speed and μ is the shear modulus. We calculate the stress transfer functional $f(x,t)$ using a spectral method [*Perrin et al.*, 1995; *Geubelle and Rice*, 1995], and use the displacement formulation of this method. Note that although the radiation damping term is present in Eq. (20), our method of computing $f(x,t)$ accounts for the full elastodynamic response and does not result in a quasidynamic model.

Periodic boundary conditions are imposed on the fault. To prevent replicas of the rupture from affecting the solution, we place strong frictional barriers to rupture at the outer edge of the fault (the darkest shade of gray in Fig. 6). For the SW law, this barrier is defined by a large value of the yield stress. For the DR and FV laws, the barrier is obtained by increasing the value of A. The specifics of the outer fault barriers do not affect the solution we calculate on the portion of the fault that can rupture. Integration in time is achieved using a second order Runge-Kutta scheme [*Lapusta et al.*, 2000].

Previously, *Lapusta et al.* [2000] confirmed that simulations of anti-plane elastodynamic ruptures with the DR law are numerically stable. They identified a critical cell size h^* for velocity-weakening friction parameters, with

$$h^* = \frac{\gamma \mu L}{B - A}. \tag{21}$$

Ruptures were numerically stable if the spatial grid spacing dl was much smaller than h^*. The model-dependent γ is a constant of order unity, and μ is the shear modulus. For in-plane ruptures, the same expression applies with the shear modulus μ replaced by the expression $\mu/(1-\nu)$, where ν is Poisson's ratio [*Rice et al.*, 2001]. For our analysis, we can extend these results to the FV law, but because the length scale $L_{\rm FV}$ is slip rate dependent, we must replace L in Eq. (21) with the minimum of $L_{\rm FV}$ over all slip rates to determine the critical cell size for FV law ruptures. From Eq. (19), we determine that the smallest value of $L_{\rm FV}$ occurs at the smallest value of the free volume. In single event rupture calculations, this is the initial value of the free volume at $t = 0$. We choose a spatial grid spacing dl that satisfies $h^*/dl = 40$ and this choice gives well-resolved simulations. Parameters for our simulations are given in Table 1 unless otherwise noted.

Shear stress in ruptures utilizing the DR and FV laws does not have explicit dependence on slip. Instead, the slip dependence of shear stress is deduced from dynamic rupture simulations, which was done for the DR law by *Okubo* [1989] and *Bizzarri and Cocco* [2003]. In Fig. 7 we show how stress weakens as a function of slip for each law at a point 4 km from the hypocenter. We only plot the portion of the curve where the stress is weakening, and for slip beyond the range of the plot the stress is constant in the SW law and relatively constant (increasing slightly due to dynamic re-strengthening) in the DR and FV laws. The linear slip weakening law follows the prescribed curve, as expected. The DR law weakens linearly with slip, and the slip required for the DR law to reach its minimum stress is larger than $L_{\rm DR}$, as noted by *Bizzarri and Cocco* [2003]. The ratio between the total slip required to reach the minimum shear stress and $L_{\rm DR}$ is about 15, which corroborates the results of *Cocco and Bizzarri* [2002] and *Lapusta and Rice* [2003a]. The DR law matches the SW law nearly identically – this close match is a deliberate result of our choice of the friction parameters which equates the peak stress and the area under each curve for the first meter of slip. The cutoff at one meter was chosen to be larger than the amount of slip needed to reach the minimum shear stress. The area under the plot of shear stress as a function of slip determines the energy lost to frictional dissipation per unit area (the combination of fracture energy and shear heating). Matching the area under the stress versus slip curve for each law is motivated by the fact that earthquake fracture energies are the most reliable frictional quanitity that can be estimated from ground motion observations [*Guatteri and Spudich*, 2000]. By equating this quanity for all three laws, we assume that the partitioning of released strain energy between dissipation and seismic radiation is the same.

The FV law exhibits weakening that differs significantly from the other laws. During the initial phases of slip (i.e. at low slip rates), the length scale $L_{\rm FV}$ is relatively small, and consequently stress weakens rapidly with slip. The length scale $L_{\rm FV}$ increases at larger slip rates, and as a result the curve exhibits an increasingly gentle slope once the fault begins to slip more rapidly. Compared to the DR and SW laws, the initial onset of weakening occurs more rapidly for the FV law, while the total slip distance over which the fault weakens is ultimately larger.

Both the FV and DR laws have a slip-hardening phase as slip initiates. The duration of slip-hardening is very short, only lasting for the first few millimeters of slip in both the FV and DR laws, and it is difficult to see in Fig. 7. The peak stress is reached at a slip of 1.04 mm for the FV law and 3.32 mm for the DR law. This difference is due to the smaller length scale in the FV law at low slip rates. However, $L_{\rm FV}$ is smaller than $L_{\rm DR}$ by approximately a factor of two at small slip rates, indicating that the duration of slip hardening does not scale linearly with the length scale in the friction law.

Time histories of the dynamics on the fault at a point 4 km from the hypocenter are shown in Fig. 8. With the chosen parameters each friction law supports ruptures that are expanding cracks. Note that an expanding crack is a rupture in which there is no healing during the expanding phase of the slip. Instead, the rupture grows, and slip ceases only after encountering the boundary. In contrast, a self-healing pulse corresponds to a narrow rupture where healing occurs shortly after the arrival of the rupture front.

The slip rate plots in Fig. 8 illustrate the crack-like nature of the earthquake simulation with all friction laws. The DR and SW laws are nearly identical in the dynamic evolution of slip rate and shear stress, confirming the results of *Bizzarri et al.* [2001]. As in Fig. 7, this is an intentional consequence of our parameter choices. The DR rupture front arrives slightly earlier than that of the SW law. Other than this difference, the SW and DR laws exhibit nearly identical time histories for both slip rate and shear stress. The rupture front arrives earliest in the FV law; this is due to the smaller value of $L_{\rm FV}$ at nucleation slip velocities. The FV law also exhibits lower peak slip rates. The difference in the peak slip rate is due to the largest slip rates occurring just prior to the shear stress reaching its minimum value. While the stress is decreasing, stored elastic energy is released and slip accelerates. Throughout this process, the more rapidly the shear stress weakens, the larger the slip acceleration. For the FV law, the rate that stress weakens with slip is not uniform, which means that slip accelerates very rapidly at first, and less rapidly as the weakening rate decreases. The weakening rate of the FV law rupture is lower than that of the DR or SW law ruptures when the ruptures reach their peak slip rate. Consequently, the maximum slip rate for the FV law rupture is smaller.

State variable evolution is similar for the FV and DR laws. Arrival of the crack tip causes a period of rapid dilation followed by more gradual compaction for the FV law. The contact lifetime in the DR law drops very rapidly initially, and grows slightly on the crack interior. The minimum shear stress in each law corresponds to the maximum value of the free volume in the FV law or the minimum contact lifetime in the DR law.

For in-plane ruptures, an important distinction between the friction laws arises in the context of supershear ruptures. The in-plane geometry permits rupture velocities faster than the shear wave speed, confirmed in simulations by *Andrews* [1976b] and laboratory experiments by *Rosakis et al.* [1999]. Supershear ruptures radiate seismic waves away from the fault in a different manner than subshear ruptures [*Dunham and Archuleta*, 2005], and seismic records give evidence for supershear rupture velocites in several earthquakes [*Archuleta*, 1984; *Bouchon et al.*, 2001; *Dunham and Archuleta*, 2004].

The nucleation length of the friction law influences the transition to supershear. Sub-Rayleigh ruptures radiate shear waves ahead of the crack tip on the fault. If the stress peak due to this shear wave is large enough, it can initiate unstable slip that propagates faster than the shear wave speed. For matching frictional dissipation, the FV law has a smaller nucleation length. Given identical initial shear loads and frictional dissipation, the smaller nucleation length can allow a supershear transition to occur for the FV law when a DR rupture remains sub-Rayleigh. This phenomena is illustrated in Fig. 9. These plots show the spatio-temporal evolution of slip rate for both the FV and DR friction laws. Both ruptures start out as expanding sub-Rayleigh cracks, and the smaller nucleation length for the FV law enables a transition to supershear rupture. A crack-like rupture is maintained throughout fault slip for both friction laws.

Fixing all model parameters except for the initial shear stress τ_{load} and the length scale at nucleation slip rates (the value of L_{FV} at the initial free volume, or L_{DR}), we generate a diagram which distinguishes between when the rupture transitions to supershear versus when it remains sub-Rayleigh. The length scale in the DR law is varied by changing l. Note that the intial value of the state variable depends on l ($\theta(t=0) = l/V_1$), and this is also altered by changes in l. The length scale in the FV law is altered by changing the dilation coefficient α and the compaction rate R_c, keeping the relative maginitude of dilation and compaction α/R_c fixed (the steady-state friction depends on only the combination α/R_c). All other parameters in Table 1 remain fixed for all simulations. The nucleation patch is the same in every simulation. The differences in the supershear transition between the DR and FV laws are independent of the nucleation procedure.

The resulting diagrams are shown in Fig. 10 with the horizontal axis showing either (a) the frictional energy dissipated per unit area at a point 4 km from the hypocenter in the first meter of slip, or (b) L at nucleation slip rates. The vertical axis is the initial shear load τ_{load} in both plots. Points on each plot are the largest value of the (a) dissipated energy per area or (b) L at which unstable supershear rupture was observed in our simulations. Above and to the left of these points, the crack will propagate faster than the shear wave speed. Growth of ruptures for conditions below and to the right are confined to sub-Rayleigh speeds. Plot (a) confirms more systematically what was observed in Fig. 9. Given equal frictional energy dissipation, for a range of initial shear loads the FV law can nucleate supershear rupture when the DR law cannot. If L at nucleation slip rates is matched between the two laws, the reverse is true and ranges of parameters exist where the DR law permits transition to supershear which is absent for the FV law. However, in this case the frictional energy dissipated is much greater for the FV law because of the velocity dependence of L_{FV} which takes its smallest value at the onset of rupture.

4. Rapid Weakening

There is increasing experimental evidence that friction at rapid slip velocities is lower than what would be predicted by extrapolating the DR law to seismic slip velocities [*Tsutsumi and Shimamoto*, 1997; *Tullis and Goldsby*, 2003; *Di Toro et al.*, 2004; *Hirose and Shimamoto*, 2005; *O'Hara et al.*, 2006]. Many earthquake modelers adapt constitutive laws that weaken rapidly with velocity to account for the weakening observed in the laboratory. Neither the DR law nor the FV law considered in the previous section incorporates weakening which is faster than logarithmic with slip rate. Both laws must be modified to account for rapid weakening. In this section, we develop the rapid weakening constitutive laws and implement them into dynamic rupture simulations to assess how the slip rate dependence of L_{FV} impacts dynamic ruptures that weaken more rapidly than logarithmically with slip rate.

Recently, *Rice* [2006] introduced a modification of the DR law based on flash heating at asperity contacts. The modified DR law allows for rapid velocity weakening at higher slip rates. The modification is implemented using a phenomenological correction factor which provides a crossover from weakening logarithmically at small slip rates to weakening as $1/V$ at seismic slip rates. The characteristic slip rate V_W at which this functional change in weakening occurs is estimated based on thermodynamic calculations to be 0.1-1 m/s [*Rice*, 2006]. The discussion in *Rice* [2006] focused mainly on the steady-state friction at high slip rates, while the actual friction law used in simulations [*Lapusta and Rice*, 2003b] matches the one we present here.

The phenomenological correction for flash heating to the DR law results in a modification to Eq. (2) of the form

$$\tau = \frac{\sigma \left[f_0 + a \log \left(V/V_0 \right) + b \log \left(\theta V_0 / l \right) \right]}{1 + l/V_W \theta}. \qquad (22)$$

The law maintains the ageing evolution law for the state variable θ, Eq. (3). For our rapid weakening simulations with the DR law, Eq. (22) is used as the constitutive model for the fault. This modifies the steady-state friction so that

$$\tau_{ss} = \frac{\sigma \left[f_0 + (a-b) \log \left(V_{ss}/V_0 \right) \right]}{1 + V_{ss}/V_W}. \qquad (23)$$

The DR flash heating law at steady state (Eq. (23)) introduces the factor $(1 + V_{ss}/V_W)^{-1}$ to the friction law, which modifies the friction at the large slip rates when heating of asperity contacts becomes significant. This law has been used in dynamic rupture calculations. For low loading stresses, the DR law with flash heating tends to produce ruptures that are self-healing pulses rather than expanding cracks [*Zheng and Rice*, 1998]. It has been suggested that earthquakes propagate as self-healing pulses [*Heaton*, 1990]. In order to compare the DR and FV laws in this regime, we alter the FV law to allow rapid weakening which can also lead to pulse-like rupture. We modify the FV law to match the functional form of the steady-state velocity weakening in the DR flash heating model (Eq. (23)).

Three changes to the FV law are necessary to construct a version that matches the additional factor $(1 + V_{ss}/V_W)^{-1}$ in the DR flash heating law at steady-state. The modification to the FV law to account for rapid weakening changes three of the equations, all of which can be found in the derivation in Appendix A. The first modification involves the rates at which STZs reverse (Eq. (31)), and the other

two changes involve the dynamic equations for the STZ populations (Eq. (37)-(38)) to prevent the number of STZs from diverging at high slip rates. For the STZ reversal rates $R_{\pm}$, we include an extra free volume-dependent factor. The STZs reverse at a much greater rate when the fault dilates at high slip rates. The modified STZ flipping rates, which replace Eq. (31) are

$$R_{\pm} = R_0 \exp\left[-E_a/kT \pm \tau/\sigma_d - \chi_s/\chi \pm \frac{R_c}{\alpha\sigma_d V_W}\exp\left(-\chi_c/\chi\right)\right]. \quad (24)$$

The additional factor is specifically chosen to give the same steady-state velocity dependence used in the flash heating model, Eq. (23). To prevent the STZ bias Δ from diverging at high slip rates, we modify Eq. (37) to read

$$\frac{d\Delta}{dt} = \frac{V}{\epsilon_0}\left\{1 - \frac{\left[\tau + \frac{R_c}{\alpha V_W}\exp\left(-\chi_c/\chi\right)\right]}{\tau_0}\Delta\right\}. \quad (25)$$

Finally, the dynamical equation for the total number of STZs (Eq. (38)) must be changed to be consistent with the new equation for the STZ bias:

$$\frac{d\Lambda}{dt} = \frac{\left[\tau + \frac{R_c}{\alpha V_W}\exp\left(-\chi_c/\chi\right)\right]V}{\tau_0\epsilon_0} \times \left[\exp\left(-\chi_h/\chi\right) - \Lambda\right]. \quad (26)$$

The other equations in the FV law remain unchanged (Eq. (30) for the shear strain rate and Eq. (15) for free volume evolution).

As in the FV law without rapid weakening, the STZs distinguish between locked and slipping solutions to the constitutive equations. The variable m_{RW} is introduced to either lock the fault or set the STZ populations to their steady-state value. The rapid weakening friction law that we adopt for dynamic rupture simulations is

$$V = V_* \exp\left[-f_* - \left(\chi_s + \chi_h\right)/\chi\right]\left(1 - m_{RW}\right) \times \sinh\left[\tau/\sigma_d + \frac{R_c}{\alpha\sigma_d V_W}\exp\left(-\chi_c/\chi\right)\right]; \quad (27)$$

$$\frac{d\chi}{dt} = -R_c \exp\left(-\chi_c/\chi\right) + \alpha\tau V. \quad (28)$$

These correspond to Eq. (14)-(15) modified for rapid weakening. For the rapid weakening FV law the variable m_{RW} is given by:

$$m_{RW} = \begin{cases} 1, \\ \quad [\tau \le \tau_0 \exp\left(\chi_h/\chi\right) - \frac{R_c}{\alpha V_W}\exp\left(-\chi_c/\chi\right)]; \\ \tau_0 \exp\left(\chi_h/\chi\right) / \left[\tau + \frac{R_c}{\alpha V_W}\exp\left(-\chi_c/\chi\right)\right], \\ \quad [\tau > \tau_0 \exp\left(\chi_h/\chi\right) - \frac{R_c}{\alpha V_W}\exp\left(-\chi_c/\chi\right)]. \end{cases} \quad (29)$$

The variable m_{RW} sets the STZs to their steady-state value when the fault is slipping, and locks the fault below the yield stress.

In addition to modifying the steady-state velocity dependence to account for rapid weakening, the alterations to the FV law have the advantage of preventing the free volume from diverging at high slip rates so that unlike the original FV law, the rapid weakening version has steady-state solutions for all slip velocities. The length scale $L_{\rm FV}$ increases with slip velocity as before.

Friction parameters used in rapid weakening simulations are listed in Table 2. For both laws, rapid weakening leads to a decrease in the critical cell size h^* due to increased $B - A$ at high slip rates, so numerically stable simulations require a smaller grid spacing.

Figure 11 shows the time histories of slip velocity, shear stress, and the appropriate state variable for anti-plane ruptures governed by the rapid weakening FV and DR laws. Each quantity is measured at a point 1.5 km from the hypocenter on a 6 km long fault. A low loading stress $\tau_{\rm load}$ = 22 MPa promotes rupture in the form of a self-healing slip pulse for both choices of the constitutive law. A brief pulse of rapid slip heals and quickly recovers shear stress once the fault locks. We note that the free volume dilates more rapidly than the FV law without rapid weakening, and the free volume has little variation over a large range of slip velocities.

A plot of shear stress as a function of slip for each law at a point 1.5 km from the hypocenter is shown in Fig. 12. As before the DR law, now with flash heating, differs from the FV law, now with rapid weakening, in the slip rate dependence of the length scale $L_{\rm FV}$ in contrast to the constant $L_{\rm DR}$. Parameters are selected for equal slip in ruptures with each law. When slip is fixed in this manner the DR law dissipates more frictional energy. As with the ruptures without rapid weakening, the FV law requires additional slip to weaken to its minimum shear stress. The nucleation length is smaller for the FV law, so the DR flash heating law requires an increase in the DR b parameter for both laws to permit rupture for an identical initial shear load.

Snapshots of the slip rate as a function of position along strike for an anti-plane rupture with the rapid weakening FV law are shown in Fig. 13. This illustrates how the rupture grows in both space and time. The plots indicate that the rupture starts out as a crack-like rupture before it transitions to a self-healing pulse-like rupture. The DR law with flash heating produces ruptures with similar slip rates and pulse spatial widths, although the slipping front takes longer to reach the fault boundary than in the FV law with rapid weakening.

For in-plane ruptures, the initial shear load determines whether the earthquake ruptures as a self-healing pulse, an expanding crack limited by the Rayleigh wave speed, or a supershear crack. The diagram in Fig. 14 shows which mode occurs as a function of the initial shear load and frictional energy dissipation for the FV and DR laws with rapid weakening. The frictional energy dissipated per area in the first meter of slip at a point 1.5 km from the hypocenter is plotted on the horizontal axis, and the initial shear load is plotted on the vertical axis. Results for the FV (DR) law are plotted as plusses (squares) for the sub-Rayleigh/supershear transition and circles (triangles) for the crack/pulse transition. Each point on the plot corresponds to the smallest initial stress permitting supershear crack propagation for the sub-Rayleigh/supershear transition, or the smallest initial stress for which pulse-like rupture is not observed for the crack/pulse transition.

For the lowest stresses, pulse-like rupture limited by the Rayleigh wave speed occurs. The stress at which the ruptures transition from pulses to expanding cracks is independent of the amount of frictional dissipation within a given law. However, the DR law requires a smaller initial shear stress to rupture as a self-healing pulse, despite the fact that the two laws have identical velocity weakening in steady-state. The difference arises because the DR law attains a lower dynamic sliding stress (Fig. 12). The dynamic friction determines the initial shear stress at which the transition to pulse-like rupture occurs [*Zheng and Rice*, 1998]. Here the steady-state velocity weakening rate in the friction law is of primary importance, as the DR and FV rapid weakening laws both transition to pulse-like rupture at similar stresses. However, because the functional form of the steady-state velocity weakening is identical in the FV and DR rapid weakening laws, the difference in the initial stresses at which the

crack/pulse transition occurs in Fig. 14 is due to the stress weakening differently with slip in the two friction laws.

At intermediate values of the initial load a sub-Rayleigh expanding crack solution exists. At higher stresses the crack transitions to supershear rupture velocities. Both the FV and DR rapid weakening laws show that the stress at which the transition to supershear occurs depends on the amount of frictional dissipation. Comparing the two laws, the sub-Rayleigh/supershear transition appears nearly identical on the scale of Fig. 14, with approximately 0.5 MPa difference between the curves (similar to the difference in the sub-Rayleigh/supershear transition for the laws without rapid weakening, Fig. 10, where the difference appears more pronounced because of the expanded scale). This is partly due to increasing the DR b parameter to decrease the nucleation length in the DR rapid weakening law, which diminishes the nucleation length discrepancy relative to that in the laws without rapid weakening. However, we note that for the laws without rapid weakening, the faults are loaded within several MPa of failure. Therefore, a difference of 0.5 MPa in the initial load is a significant fraction of the strength excess, and the strength excess is crucial in determining if a rupture can transition to supershear. For the laws with rapid weakening, the fault is loaded tens of MPa from failure, and a difference of 0.5 MPa in the initial load is less important. The vertical scale on each of the plots reflect this difference in the strength excess between the laws with or without rapid weakening (the scale in Fig. 10 is about 10 times smaller than the scale in Fig. 14).

The rupture type plot indicates that when comparing the DR and FV rapid weakening laws, the most significant difference is associated with how the shear stress weakens with slip and not the nucleation length. The distinct forms in which stress weakens with slip for the FV and DR laws results in an increase of 4 MPa in the stress at which the crack/pulse transition occurs for the FV law with rapid weakening compared to the DR law with rapid weakening. The DR law with rapid weakening has a larger nucleation length, but the difference is small enough that the sub-Rayleigh/supershear transition occurs at roughly the same initial stress relative to the strength excess in rapid weakening laws.

5. Discussion

Our comparisons between the FV law, DR law, and SW law show that the slip rate dependence of L_{FV} impacts many properties of dynamic ruptures. These properties include the manner in which stress weakens with slip, the peak slip rate attained during rupture, and the stress at which supershear rupture is nucleated. The slip rate dependence of L_{FV} is also important in ruptures with constitutive laws that are modified to allow rapid weakening. The rapid weakening laws result in dynamic ruptures that are self-healing pulses with low initial shear stress which transition to pulse-like rupture at different initial shear stresses for the FV and DR laws with rapid weakening.

Because friction laws have implications at all scales of earthquake rupture, we discuss our results in the context of these various scales. At each scale of the earthquake problem there are uncertainties and modeling challenges. A primary objective of those working on earthquake source physics is to use mechanisms and constraints from statistical physics, material science, and rock mechanics to reduce the uncertainty and produce sharper bounds on the range of behavior that might be observed. However, even under controlled laboratory conditions friction, fracture, and deformation remain active areas of research and lack a complete microscopic description. Our hope is that a multiscale approach that investigates macroscopic consequences in parallel with microscopic mechanisms will provide insights spanning a broad range of scales.

At the scale of faults, friction laws control the complexity of individual ruptures and the associated ground motion. Models of the earthquake source are complicated by uncertainties involving the stress level on earthquake faults [*Hickman*, 1991; *Sibson*, 1994], how shear stress weakens with slip during rupture [*Abercrombie and Rice*, 2005], and the energy balance of faulting [*Kanamori and Heaton*, 2000]. Additionally, while earthquake records have been inverted for constitutive parameters [*Ide and Takeo*, 1997; *Guatteri et al.*, 2001], these studies estimate slip-weakening distances that are much larger than the total slip in smaller earthquakes (d_c of order 1 m in Fig. 1). This makes it difficult to estimate the correct constitutive parameters. Comparing friction laws in the context of earthquake ruptures helps determine what macroscopic observables, such as peak ground velocity and radiated seismic energy, can be affected by these uncertainties. The FV law and the DR law produce different peak slip rates in our calculations. This will likely affect the peak ground velocity predicted in the vicinity of the fault for each law [*Aagaard et al.*, 2001]. Additionally, our modeling indicates that the FV law and DR law transition to supershear at different shear loads for a given frictional dissipation. Supershear rupture velocities radiate shear waves that do not attenuate with distance from the fault [*Dunham and Archuleta*, 2005], and thus supershear rupture can affect the spatial extent of regions with high ground velocities.

On a smaller scale, the aggregate behavior of gouge influences the dynamics of friction. This scale can be studied in the laboratory and through numerical simulations. The FV law ties weakening and re-strengthening to dilation and compaction, and predicts a slip rate dependence of L_{FV} that is absent in the DR law. The FV law closely matches the slip rate dependence of L observed by *Mair and Marone* [1999] for sheared granular layers. For bare granite surfaces, little variation in L is observed over slip rates ranging from 10^{-2} to $10^{3.5}$ μm/s by *Blanpied et al.* [1998]. Because the rate dependence of the length scale L_{FV} is due to dilation, the amount of dilation of the sheared layer determines how much variation in the length scale will occur. The *Blanpeid et al.* experiments use relatively smooth granite surfaces, which dilate less than a rough surface or a layer of gouge. The FV law would thus predict less variation in the length scale L_{FV} for these experiments. Dilation with increasing slip rate is observed in rock mechanics experiments [*Marone and Kilgore*, 1993; *Mair and Marone*, 1999] and boundary lubrication experiments [*Drummond and Israelachvili*, 2000]. However, the dilatancy of real faults during rapid seismic slip is unknown. Large overburden pressures may not allow for significant dilation. Previous studies have added observed laboratory porosity evolution to the DR framework [*Segall and Rice*, 1995; *Sleep*, 1995]. The FV law differs from other models of dilation and compaction in that it ties velocity weakening directly to dilation and compaction of the gouge layer. The porosity models in the DR framework maintain a length scale that does not vary with slip rate, which is different than the evolution predicted by the FV law. In numerical studies, STZ theory compares favorably with molecular dynamics simulations of amorphous materials [*Falk and Langer*, 1998, 2000] and with contact dynamics simulations of granular materials [*Lois et al.*, 2005].

At this smaller scale, the collective motion of gouge particles form the basis for constitutive laws. The FV law assumes that the deformation of the gouge is well approximated by mean-field theory at this scale (i.e., shear strain is assumed to be uniform within the gouge layer). However, strain localization within a layer of fault gouge is observed in numerical simulations [*Morgan and Boettcher*, 1999], laboratory experiments [*Marone*, 1998], and natural faults [*Chester and Chester*, 1998]. The mean-field assumption of the FV

law may omit crucial friction dynamics that occur when strain localizes. *Manning et al.* [2007] studied strain localization in STZ theory, and found that localization influences the transient stress dynamics. Resolving the structure within the gouge layer, as well as analyzing the response of this structure to continued deformation, are needed to fully understand the mechanics of fault gouge and its influence on rupture dynamics. *Daub et al.* [2008] implemented STZ Theory with strain localization into dynamic rupture models, and found that localization is a mechanism for enhancing the velocity weakening of faults. Their simulations resulted in dynamic ruptures with increased stress drops and peak slip rates, revealing that small scale properties of gouge deformation affect fault-scale rupture.

An alternative formulation of STZ theory replaces the free volume evolution law with local variations in the STZ density governed by an effective temperature [*Langer*, 2008]. Larger values of the effective temperature indicate larger disorder and a local increase in the number of STZs. The effective temperature version of the STZ equations does not include an activation volume as in the expressions for $R_{\pm}$ (Eq. (31)) that increases the rate at which STZs flip. Rather, a larger number of STZs form to allow for more rapid plastic shear strain in the gouge. The effective temperature follows a slightly different evolution equation than the free volume, but otherwise the effective temperature formulation retains a form nearly identical to the FV law presented here. For this study, we use a free volume dependent version of STZ theory that incoporates dilation and compaction, which have been directly observed in laboratory experiments on fault gouge. Future work with STZ theory will compare free volume and effective temperature.

At the smallest scales, individual grain contacts and associated wear, heating, fracture and deformation determine the most basic interactions for fault friction. Establishing the physical interactions that are the most important at the high pressures and slip rates of earthquake rupture is an active area of research in earthquake source physics. Because the physics of granular and amorphous systems are not fully understood, determining the consequences of these microscopic interactions for earthquake rupture remains a challenge. The FV law begins with a more microscopic picture than other constitutive laws, though many of the possible more complicated microscopic features are still ignored. Fault zones contain pore fluids, which influence fault healing [*Frye and Marone*, 2002], and can become pressurized due to shear heating [*Lachenbruch*, 1980]. How contacts adhere, heal, and regain strength has tremendous implications for fault re-strengthening and earthquake recurrence over a broad range of temporal scales [e.g., *Dieterich*, 1972; *Marone et al.*, 1995; *Li et al.*, 2003] – a granular description of fault gouge where only contact forces are relevant is only the beginning of a microscopic description of fault zones. We expect many of these other effects will be important, especially on the time scale of earthquake recurrence. STZ Theory was initially formulated in the context of amorphous solids with more complicated particle interactions than those which arise for granular materials [*Falk and Langer*, 1998, 2000]. Interestingly, the STZ equations which describe the other amorphous materials are the same as those for granular materials, suggesting that there are at least some features in this class of systems which may be universal. However, none of these theories incorporate the full range of complex interactions which are likely to occur in gouge. While the FV law begins to link microscopic physics to fault scale behavior, the greater variety of grain-scale physics need to be incorporated into future constitutive models to fully capture the complex dynamics occuring in fault zones during the seismic cycle.

6. Appendix A: Derivation of the Free Volume Law

The Free Volume law begins with Shear Transformation Zone (STZ) Theory, which was introduced by *Falk and Langer* [1998, 2000] to describe fracture and deformation of amorphous materials. We consider a layer of fault gouge that may deform inelastically in small, localized regions. These regions are called shear transformation zones (STZs). Here, plastic strain designates all deformation in the gouge that is not elastic. STZ rearrangements are the lone source of inelastic strain in the FV law. The shear strain rate for this inelastic deformation is a function of the number of STZs in the gouge, the applied shear stress, and the density of the gouge. Density changes are due to dilation and compaction, and are modeled by the evolution of a dynamic state variable representing the free volume in the gouge layer. The shear strength of the gouge weakens as the fault dilates, and regains strength by compacting. The number of STZs and the free volume are dynamic state variables in the FV law. An alternative formulation of STZ constitutive laws use an effective temperature (i.e. local disorder) in place of the free volume [*Langer*, 2008]. We discuss this interpretation in Section 5.

STZs are assumed to have two distinct orientations, designated "+" and "−." These designate the two possible metastable STZ configurations, each one corresponding to one of the principal stress axes. The picture at the left in Fig. 3 is in the "+" configuration and is aligned with the smallest principal stress, and the picture at the right has flipped to the "−" orientation and is now aligned with the largest principal stress. An STZ in the "+" orientation can switch to the "−" orientation and increase the plastic shear strain. This deformation is potentially reverisble: the "−" orientation can change to a "+" orientation, though under the large stresses of seismic faulting this occurs infrequently. When the gouge is flowing, STZs are constantly created and destroyed in both orientations. Plastic shear strain accumulates in the gouge through the following sequence: flow creates "+" STZs, the "+" STZs flip to the "−" orientation, the gouge flow destroys the "−" STZs, and new "+" STZs form to repeat the cycle.

Quantitatively, the number of STZs in each orientation are denoted by n_+ and n_-. The rates at which the STZs reverse are R_+ and R_-. The plastic shear strain rate $D_{\rm pl}$ is proportional to the net sum of all reversing STZs:

$$D_{\rm pl} = D_0 \left(R_+ n_+ - R_- n_- \right). \tag{30}$$

The accumulated strain per STZ reversal is D_0. For simplicity, we assume that the STZs are uniformly distributed throughout the material. Thus only the total number of each population is relevant.

The rates $R_{\pm}$ depend on the shear stress τ and the local density of the deforming material. Density is incorporated in the model by including a variable free volume χ. The free volume is a dimensionless, intensive quantity that describes the packing of the gouge. We assume the following form for $R_{\pm}$:

$$R_{\pm} = R_0 \exp\left(-E_a/kT \pm \tau/\sigma_d - \chi_s/\chi\right). \tag{31}$$

Other parameters include the STZ reversal activation stress σ_d, a typical free volume required for an STZ reversal to occur χ_s, the activation energy each STZ requires to flip E_a, Bolzmann's constant k, the absolute temperature T, and the underlying attempt frequency R_0. The exponential stress dependence assumes the rate is given by an Eyring model [*Eyring*, 1936]. The free volume dependence taken here is based on the assumption that the empty voids in the material are Poisson distributed. In general, the reference

free volume for shearing χ_s depends on the shape and size distribution of the constituents composing the material.

Equations (30) and (31) define the frictional strength of the material. Dynamical equations for the number of STZs $n_\pm$ and the free volume χ complete the constitutive model. Free volume evolves according to

$$\frac{d\chi}{dt} = -R_c \exp\left(-\chi_c/\chi\right) + \alpha_d \tau D_{\rm pl}. \tag{32}$$

We include terms for compaction and dilation of the free volume. Compaction occurs at a rate determined by R_c and the value of the free volume χ relative to the characteristic free volume for compaction χ_c. The free volume dependence of the compaction term assumes that voids are Poisson distributed. A fraction of the frictional dissipation causes the material to dilate, and the coefficient α_d sets the scale for this effect. Because the rate at which frictional work is done increases with slip rate, the gouge will dilate more as the slip rate increases. As with the reference free volume for shearing χ_s, the specifics of the material determine the reference free volume for compaction χ_c. Shearing and compaction of the gouge require distinct rearrangements, and we will see their relative values determine whether the gouge is velocity strengthening or velocity weakening in steady-state.

The STZ populations can reverse orientation, and the mean flow creates and destroys STZs. The dynamical equations for the number of STZs in each orientation $n_\pm$ are

$$\begin{aligned}\frac{dn_\pm}{dt} &= R_\mp n_\mp - R_\pm n_\pm \\ &\quad + \tau D_{\rm pl}\left[A_c \exp\left(-\chi_h/\chi\right) - A_a n_\pm\right].\end{aligned} \tag{33}$$

Parameters A_c and A_a determine the rate at which the mean flow creates and annihilates STZs, respectively, and χ_h is the free volume needed to create an STZ. The reference free volume for STZ creation χ_h will typically be smaller than the free volume needed for shearing (χ_s) and compaction (χ_c).

Following *Falk and Langer* [1998, 2000], we rescale the STZ populations using a reference STZ population $n_\infty = 2A_c/A_a$:

$$\Delta = \frac{n_- - n_+}{n_\infty}, \text{ and } \Lambda = \frac{n_+ + n_-}{n_\infty}. \tag{34}$$

The total number of STZs is determined by Λ, while the bias is quantified by Δ.

Earthquake ruptures are represented in terms of the slip velocity V rather than the plastic shear strain rate $D_{\rm pl}$. Thus, we substitute $V = 2wD_{\rm pl}$, where w is the thickness of the sheared layer (slipping zone). The remaining parameters are scaled as follows: $f_* = E_a/kT$ determines the overall value of friction, $V_* = wD_0R_0A_a/A_c$ is a reference slip rate, $\alpha = \alpha_d/2w$ is the scaled dilatancy coefficient, $\epsilon_0 = 2wD_0A_c/A_a$ is the time scale for STZ reversals, and $\tau_0 = 1/(D_0A_c)$ is a stress scale for STZ reversals. We simplify the resulting equations by assuming that for seismic faulting, the stress τ is much larger than the characteristic stress fluctuations σ_d. For stresses measured in laboratory experiments on simulated faults, this is a good approximation. The resulting constitutive equations are

$$V = V_*\left[\exp\left(-f_* - \chi_s/\chi\right)\right](\Lambda - \Delta)\sinh\left(\tau/\sigma_d\right); \tag{35}$$

$$\frac{d\chi}{dt} = -R_c \exp\left(-\chi_c/\chi\right) + \alpha\tau V; \tag{36}$$

$$\frac{d\Delta}{dt} = \frac{V}{\epsilon_0}\left(1 - \frac{\tau}{\tau_0}\Delta\right); \tag{37}$$

$$\frac{d\Lambda}{dt} = \frac{V\tau}{\epsilon_0\tau_0}\left[\exp\left(-\chi_h/\chi\right) - \Lambda\right]. \tag{38}$$

The constitutive law admits solutions that are jammed ($V = 0$) if the STZ bias and total number of STZs are equal ($\Lambda = \Delta$). This means that all of the STZs are in the "$-$" orientation. If the total number of STZs Λ is larger than the bias Δ, then the gouge is flowing and the fault slips. Differentiating between the locked and slipping regimes is the principal role of the STZ dynamics, as the STZs rapidly equilibrate since they flip much faster than the time scale for free volume evolution. Therefore, it is a good approximation to regard the STZ dynamics as instantaneous, in which case the STZs provide a physical mechanism to lock the fault for jammed solutions. We set the STZ population sizes in Eq. (35) to their steady state values in the flowing regime ($\Delta = \tau_0/\tau$, $\Lambda = \exp(-\chi_h/\chi)$) to obtain Eq. (39). The locked and flowing STZ solutions are incorporated using the variable m_0:

$$\begin{aligned}V &= V_*\exp\left[-f_* - \left(\chi_s + \chi_h\right)/\chi\right](1 - m_0) \\ &\quad \times \sinh\left(\tau/\sigma_d\right);\end{aligned} \tag{39}$$

$$\frac{d\chi}{dt} = -R_c \exp\left(-\chi_c/\chi\right) + \alpha\tau V. \tag{40}$$

The values that m_0 takes depend on whether the stress is above or below the yield stress, $\tau_0 \exp(\chi_h/\chi)$:

$$m_0 = \begin{cases} 1, & [\tau \le \tau_0 \exp\left(\chi_h/\chi\right)]; \\ \frac{\tau_0}{\tau}\exp\left(\chi_h/\chi\right), & [\tau > \tau_0 \exp\left(\chi_h/\chi\right)]. \end{cases} \tag{41}$$

The free volume evolution is retained (Eq. (40)), and serves as the primary state variable for the FV law in our simulations and in our comparisons with the SW and DR friction laws.

Unlike the DR law, the FV law does not admit steady-state solutions for all slip rates. To illustrate this, we note that the compaction term $-R_c \exp\left(-\chi_c/\chi\right)$ in Eq. (40) cannot be larger than $-R_c$, which corresponds to the limit obtained as the free volume approaches infinity. If the dilation term in Eq. (40) is larger than R_c (i.e. if $\alpha\tau V > R_c$), the free volume χ will increase without bound. The critical velocity V_c and critical stress τ_c at which this occurs satisfies $\alpha\tau_c V_c = R_c$. The critical stress and critical velocity also satisfy Eq. (39) with m_0 set to its slipping value in the limit that the free volume goes to infinity:

$$V_c = V_*\left[\exp\left(-f_*\right)\right]\left(1 - \frac{\tau_0}{\tau_c}\right)\sinh\left(\frac{\tau_c}{\sigma_d}\right). \tag{42}$$

The two equations for τ_c and V_c can be combined to eliminate τ_c and determine V_c. Above this critical slip rate, steady state solutions do not exist for the FV law. The divergence of the free volume at slip rates above the critical rate V_c does not present a problem for applying this law to dynamic earthquake rupture. Values of the parameters that are consistent with laboratory experiments result in a critical velocity V_c well above typical seismic slip velocities during earthquakes (for the parameters in our dynamic rupture simulations, $V_c = 164$ m/s).

7. Appendix B: Full expressions for A, $A - B$, and L for the Free Volume Law

The exact values of the quantities $A_{\rm FV}$, $(A - B)_{\rm FV}$, and $L_{\rm FV}$, calculated by applying Eq. (5)-(7) to Eq. (14)-(15), are:

$$\begin{aligned}A_{\rm FV} &= \sigma_d \tanh\left(\frac{\tau_{ss}}{\sigma_d}\right) \\ &\quad \times \left[1 + \frac{\frac{\tau_0\sigma_d}{\tau_{ss}^2}\left(\frac{R_c}{\alpha\tau_{ss}V}\right)^{\chi_h/\chi_c}\tanh\left(\frac{\tau_{ss}}{\sigma_d}\right)}{1 - \frac{\tau_0}{\tau_{ss}}\left(\frac{R_c}{\alpha\tau_{ss}V}\right)^{\chi_h/\chi_c}}\right]^{-1}\end{aligned} \tag{43}$$

$$(A-B)_{\rm FV} = \sigma_d \tanh\left(\frac{\tau_{ss}}{\sigma_d}\right) \times \left[1 - \frac{\chi_s+\chi_h}{\chi_c} - \frac{\frac{\chi_h \tau_0}{\chi_c \tau_{ss}}\left(\frac{R_c}{\alpha\tau_{ss}V}\right)^{\chi_h/\chi_c}}{1-\frac{\tau_0}{\tau_{ss}}\left(\frac{R_c}{\alpha\tau_{ss}V}\right)^{\chi_h/\chi_c}}\right] \times \left[1 + \frac{(\chi_s+\chi_h)\,\sigma_d}{\chi_c\tau_{ss}}\tanh\left(\frac{\tau_{ss}}{\sigma_d}\right) + \left(1+\frac{\chi_h}{\chi_c}\right)\frac{\tau_0\sigma_d}{\tau_{ss}^2} \times \frac{\left(\frac{R_c}{\alpha\tau_{ss}V}\right)^{\chi_h/\chi_c}\tanh\left(\frac{\tau_{ss}}{\sigma_d}\right)}{1-\frac{\tau_0}{\tau_{ss}}\left(\frac{R_c}{\alpha\tau_{ss}V}\right)^{\chi_h/\chi_c}}\right]^{-1} \quad (44)$$

$$L_{\rm FV} = \frac{\chi_{ss}^2}{\alpha\tau_{ss}\chi_c}\left\{1+\frac{(\chi_s+\chi_h)\,\sigma_d}{\chi_c\tau_{ss}}\tanh\left(\frac{\tau_{ss}}{\sigma_d}\right) \times \left[1+\frac{\frac{\chi_h\tau_0}{(\chi_s+\chi_h)\tau_{ss}}\left(\frac{R_c}{\alpha\tau_{ss}V}\right)^{\chi_h/\chi_c}}{1-\frac{\tau_0}{\tau_{ss}}\left(\frac{R_c}{\alpha\tau_{ss}V}\right)^{\chi_h/\chi_c}}\right] \times \left[1+\frac{\tau_0\sigma_d}{\tau_{ss}^2} \times \frac{\left(\frac{R_c}{\alpha\tau_{ss}V}\right)^{\chi_h/\chi_c}\tanh\left(\frac{\tau_{ss}}{\sigma_d}\right)}{1-\frac{\tau_0}{\tau_{ss}}\left(\frac{R_c}{\alpha\tau_{ss}V}\right)^{\chi_h/\chi_c}}\right]^{-1}\right\}^{-1} \quad (45)$$

Many of the terms that are ignored in the approximations (Eq. (17)-(19)) have the denominator $1-\tau_0(R_c/(\alpha\tau_{ss}V))^{\chi_h/\chi_c}/\tau_{ss}$. When the stress is only slightly above the yield stress, this expression is nearly zero and these terms are no longer negligible. Other terms are ignored because $\sigma_d/\tau_{ss} << 1$.

Acknowledgments. The authors thank Eric Dunham for providing the dynamic rupture code used in this study, and Ralph Archuleta, Gregor Hillers, and Lisa Manning for valuable discussion. Steven Day, Nicholas Beeler, and Andrea Bizzarri provided thoughtful reviews that helped clarify the manuscript. This work was supported by the James S. McDonnell Foundation, the David and Lucile Packard Foundation, NSF grant number DMR-0606092, and the Southern California Earthquake Center. SCEC is funded by NSF Cooperative Agreement EAR-0106924 and USGS Cooperative Agreement 02HQAG0008. The SCEC contribution number for this paper is 1155.

References

Aagaard, B. T., J. F. Hall, and T. H. Heaton (2001), Characterization of near-source ground motions with earthquake simulations, *Earthquake Spectra*, *17*, 177-207.

Abercrombie, R. E., and J. R. Rice (2005), Can observations of earthquake scaling constrain slip weakening?, *Geophys. J. Int.*, *162*, 406-424, doi:10.1111/j.1365-246X.2005.02579.x.

Andrews, D. J. (1976a), Rupture propagation with finite stress in antiplane strain, *J. Geophys. Res.*, *81*, 3575-3582.

Andrews, D. J. (1976b), Rupture velocity of plane strain shear cracks, *J. Geophys. Res.*, *81*, 5679-5687.

Archuleta, R. J. (1984), A faulting model for the 1979 Imperial Valley earthquake, *J. Geophys. Res.*, *89*, 4559-4585.

Bizzarri, A., and M. Cocco (2003), Slip-weakening behavior during the propagation of dynamic ruptures obeying rate- and state-dependent friciton laws, *J. Geophys. Res.*, *108*(B8), 2373, doi:10.1029/2002JB002198.

Bizzarri, A., and M. Cocco (2003), Slip-weakening behavior during the propagation of dynamic ruptures obeying rate- and state-dependent friciton laws, *J. Geophys. Res.*, *108*(B8), 2373, doi:10.1029/2002JB002198.

Bizzarri, A., and M. Cocco (2005), 3D dynamic simulations of spontaneous rupture propagation governed by different constitutive laws with rake rotation allowed, *Annals of Geophys.*, *48*(2), 279-299.

Bizzarri, A., M. Cocco, D. J. Andrews, and E. Boschi (2001), Solving the dynamic rupture problem with different numerical approaches and constitutive laws, *Geophys. J. Int.*, *143*(3), 656-678, doi:10.1046/j.1365-246x.2001.01363.x.

Blanpied, M. L., T. E. Tullis, and J. D. Weeks (1998), Effects of slip, slip rate, and shear heating on the friction of granite, *J. Geophys. Res.*, *103*(B1), 489-512, doi:10.1029/97JB02480.

Bouchon, M., M. P. Bouin, H. Karabulut, M. N. Toksöz, M. Dietrich, and A. Rosakis (2001), How fast is rupture during an earthquake? New insights from the 1999 Turkey earthquakes, *Geophys. Res. Lett.*, *28*(14), 2723-2726, doi:10.1029/2001GL013112.

Carlson, J. M., and J. S. Langer (1989), Mechanical model of an earthquake fault, *Phys. Rev. A*, *40*, 6470.

Chester, F. M., and J. S. Chester (1998), Ultracataclasite structure and friction processes of the Punchbowl fault, San Andreas system, California, *Tectonophysics*, *295*, 199-221.

Cochard, A., and R. Madariaga (1994), Dynamic faulting under rate-dependent friction, *Pure Appl. Geophys.*, *142*(3-4), 419-445.

Cochard, A., and R. Madariaga (1996), Complexity of seismicity due to highly rate-dependent friction, *J. Geophys. Res.*, *101*, 25321-25336, doi:10.1029/96JB02095.

Cocco, M., and A. Bizzari (2002), On the slip-weakening behavior of rate-and-state dependent constitutive laws, *Geophys. Res. Lett.*, *29*(11), 1516, doi:10.1029/2001GL013999.

Daub, E. G., M. L. Manning, J. M. Carlson (2008), Shear strain localization in elastodynamic rupture simulations, *Geophys. Res. Lett.*, *35*, L12310, doi:10.1029/2008GL033835.

Day, S. M. (1982), Three-dimensional simulation of spontaneous rupture: the effect of non-uniform prestress, *Bull. Seismol. Soc. Am.*, *72*, 1881-1902.

Dieterich, J. H. (1972), Time dependent friction in rocks, *J. Geophys. Res.*, *77*(20), 3690.

Dieterich, J. H. (1979), Modeling of rock friction 1. Experimental results and constitutive equations, *J. Geophys. Res.*, *84*(NB5), 2161-2168.

Dieterich, J. H., and B. D. Kilgore (1994), Direct observation of frictional contacts – new insights for state dependent properties, *Pure Appl. Geophys.*, *143*(1-3), 283-302.

Di Toro, G., D. L. Goldsby, and T. E. Tullis (2004), Friction falls towards zero in quartz rock as slip velocity approaches seismic rates, *Nature*, *427*, 436-439.

Drummond, C., and J. Israelachvili (2000), Dynamic behavior of confined branched hydrocarbon lubricant fluids under shear, *Macromolecules*, *33*, 4910-4920.

Dunham, E. M., and R. J. Archuleta (2004), Evidence for a supershear transient during the 2002 Denali fault earthquake, *Bull. Seismol. Soc. Am.*, *94*(6), 256-268, doi:10.1785/0120040616.

Dunham, E. M., and R. J. Archuleta (2005), Near-source ground motion from steady state dynamic rupture pulses, *Geophys. Res. Lett.*, *32*(3), L03302, doi:10.1029/2004GL021793.

Eyring, H. J. (1936), Viscosity, plasticity, and diffusion as examples of absolute reaction rates, *J. Chem. Phys.*, *4*, 283.

Falk, M. L., and J. S. Langer (1998), Dynamics of viscoplastic deformation in amorphous solids, *Phys. Rev. E*, *57*(6), 7192-7205.

Falk, M. L., and J. S. Langer (2000), From simulation to theory in the physics of deformation and fracture, *MRS Bull.*, *25*(5), 40-45.

Favreau, P., I.R. Ionescu, and M. Campillo (1999), On dynamic sliding with rate- and state-dependent friction laws, *Geophys. J. Int.*, *139*(3), 671-678, doi:10.1046/j.1365-246x.1999.00970.x.

Frye, K. M., and C. Marone (2002), The effect of humidity on granular friction at room temperature, *J. Geophys. Res.*, *107*(11), 2309, doi:10.1029/2001JB000654.

Geubelle, P. H., and J. R. Rice (1995), A spectral method for 3-dimensional elastodynamic fracture problems, *J. Mech. Phys. Solids*, *43*(11), 1791-1824.

Guatteri, M., and P. Spudich (2000), What can strong-motion data tell us about slip-weakening fault-friction laws?, *Bull. Seism. Soc. Am.*, *90*, 98-116, doi:10.1785/0119990053.

Guatteri, M., P. Spudich, and G. C. Beroza (2001), Inferring rate and state friction parameters from rupture models of the 1995 Hyogo-ken Nambu (Kobe) earthquake, *J. Geophys. Res.*, *106*(B11), 26511-26521, doi:10.1029/2001JB000294.

Harris, R. A., and S. M. Day (1993), Dynamics of fault interaction: parallel strike-slip faults, *J. Geophys. Res.*, *98*, 4461-4472.

Heaton, T. H. (1990), Evidence for and implications of self-healing pulses of slip in earthquake rupture, *Phys. Earth Plant. Int.*, *64*(1), 1-20.

Hickman, S. H. (1991), Stress in the lithosphere and the strength of active faults, *Rev. Geophys.*, *29*, 759-775.

Hirose, T., and T. Shimamoto (2005), Growth of molten zone as a mechanism of slip weakening of simulated faults in gabbro during fricitonal melting, *J. Geophys. Res.*, *110*(B5), B05202, doi:10.1029/2004JB003207.

Ida, Y. (1972), Cohesive force across the tip of a longitudinal-shear crack and Griffith's specific surface energy, *J. Geophys. Res.*, *77*(20), 3796-3805.

Ide, S., and M. Takeo (1997), Determination of constitutive relations of fault slip based on seismic wave analysis, *J. Geophys. Res.*, *102*(B12), 27379-27391, doi:10.1029/97JB02675.

Kanamori, H., and T. H. Heaton (2000), Microscopic and macroscopic physics of earthquakes, in *Geocomplexity and the Physics of Earthquakes*, American Geophysical Union Geophysical Monograph 120, pp. 147-163, AGU, Washington, DC.

Lachenbruch, A. H., (1980), Frictional heating, fluid pressure, and the resistance to fault motion, *J. Geophys. Res.*, *85*(NB11), 6097-6112.

Langer, J. S. (2008), Shear-transformation-zone theory of plastic deformation near the glass transition, *Phys. Rev. E*, *77*, 021502.

Lapusta, N., and J. R. Rice (2003), Nucleation and early seismic propagation of small and large events in a crustal earthquake model, *J. Geophys. Res.*, *108*(B4), 2205, doi:10.1029/2001JB000793.

Lapusta, N., and J. R. Rice (2003b), Low-heat and low-stress operation in earthquake models of statically strong but dynamically weak faults, *Eos Trans. AGU*, *84*(46), Fall Meet. Suppl., Abstract S51B-02.

Lapusta, N., J. R. Rice, Y. Ben-Zion, and G. Zheng (2000), Elastodynamic analysis for slow tectonic loading with spontaneous rupture episodes on faults with rate- and state-dependent friction, *J. Geophys. Res.*, *105*(B10), 23765-23789, doi:10.1029/2000JB900250.

Lemaitre, A. (2002), Rearrangements and dilatancy for sheared dense materials, *Phys. Rev. Lett.*, *89*(19), 195503.

Lemaitre, A., and J. M. Carlson (2004), Boundary lubrication with a glassy interface, *Phys. Rev. E*, *69*(6), 061611.

Li, Y.-G., J. E. Vidale, S. M. Day, D. D. Oglesby, and E. Cochran (2003), Postseismic fault healing on the rupture zone of the 1999 *M* 7.1 Hector Mine, California, earthquake, *Bull. Seismol. Soc. Am*, *93*, 854-869, doi:10.1785/0120020131.

Lois, G., A. Lemaitre, and J. M. Carlson (2005), Numerical tests of constitutive laws for dense granular flows, *Phys. Rev. E*, *72*, 051303.

Madariaga, R., K. B. Olsen, and R. J. Archuleta (1998), Modeling dynamic rupture in a 3D earthquake fault model, *Bull. Seismol. Soc. Am.*, *88*, 1182-1197.

Mair, K., and C. Marone (1999), Friction of simulated fault gouge for a wide range of velocities and normal stresses, *J. Geophys. Res.*, *104*(B12), 28899-28914 doi:10.1029/1999JB900279.

Manning, M. L., J. S. Langer, and J. M. Carlson (2007), Strain localization in a shear transformation zone model for amorphous solids, *Phys. Rev. E*, *76*(5), 056106.

Marone, C. (1998), Laboratory-derived friction laws and their application to seismic faulting, *Ann. Rev. Earth Planet. Sci.*, *26*, 643-696.

Marone, C., and B. Kilgore (1993), Scaling of the critical slip distance for seismic faulting with shear strain in fault zones, *Nature*, *362*(6421), 618-621.

Marone, C., J. E. Vidale, and W. Ellsworth (1995), Fault healing inferred from time dependent variations in source properties of repeating earthquakes, *Geophys. Res. Lett.*, *22*(22), 3095-3098, doi:10.1029/95GL03076.

Morgan, J. K., and M. S. Boettcher (1999), Numerical simulations of granular shear zones using the distinct element method - 1. Shear zone kinematics and the micromechanics of localization, *J. Geophys. Res.*, *104*(B2), 2703-2720, doi:10.1029/1998JB900056.

Nielsen, S. B., and J. M. Carlson (2000), Rupture pulse characterization: Self-healing, self-similar, expanding solutions in a continuum model of fault dynamics, *Bull. Seismol. Soc. Am.*, *90*, 1480-1497, doi:10.1785/0120000021.

Nielsen, S. B., J. M. Carlson, and K. B. Olsen (2000), Influence of friction and fault geometry on earthquake rupture, *J. Geophys. Res.*, *105*(B3), 6069-6088, doi:10.1029/1999JB900350.

O'Hara, K., K. Mizoguchi, T. Shimamoto, and J. C. Hower (2006), Experimental frictional heating of coal gouge at seismic slip rates: Evidence for devolotization and thermal pressurization of gouge fluids, *Tectonophysics*, *424*, 109-118.

Okubo, P. (1989), Dynamic rupture modeling with laboratory-derived constitutive relations, *J. Geophys. Res.*, *94*(B9), 12321-12335.

Perrin, G., J. R. Rice, and G. Zheng (1995), Self-healing slip pulse on a frictional surface, *J. Mech. Phys. Solids*, *43*, 1461-1495.

Rice, J. R. (1983), Constitutive relations for fault slip and earthquake instabilities, *Pure Appl. Geophys.*, *121*, 443-475.

Rice, J. R. (2006), Heating and weakening of faults during earthquake slip, *J. Geophys. Res.*, *111*, B05311, doi:10.1029/2005JB004006.

Rice, J. R., and A. L. Ruina (1983), Stability of steady frictional slipping, *J. Appl. Mech.*, *50*, 343-349.

Rice, J. R., N. Lapusta, and K. Ranjith (2001), Rate and state dependent friction and the stability of sliding between elastically deformable solids, *J. Mech. Phys. Solids*, *49*, 1865-1898,

Rosakis, A. J., O. Samudrala, and D. Coker (1999), Cracks faster than the shear wave speed, *Science*, *284*, 1337-1340.

Ruina, A. L. (1980), Friction laws and instabilities: A quasistatic analysis of some dry frictional behavior, Ph.D. Thesis, Brown University, Providence, R.I.

Ruina, A. L. (1983), Slip instability and state variable friction laws, *J. Geophys. Res.*, *88*, 10359-10370.

Scott, G. D., and D. M. Kilgour (1969), The density of random close packing of spheres, *J. Phys. D: Appl. Phys.*, *2*, 863-866, doi:10.1088/0022-3727/2/6/311

Segall, P., and J. R. Rice (1995), Dilatancy, compaction, and slip instability of a fluid-infiltrated fault, *J. Geophys. Res.*, *100*(B11), 22155-22171, doi:10.1029/95JB02403.

Shaw, B. E., and J. R. Rice (2000), Existence of contiuum complexity in the elastodynamics of repeated fault ruptures, *J. Geophys. Res.*, *105*(B10), 23791-23810, doi:10.1029/2000JB900203.

Sibson, R. H. (1994), An assessment of field evidence for "Byerlee" friction, in *Faulting, Friction and Earthquake Mechanics*, Part 1, pp. 645-662, Birkhaeuser Verlag, Basel, Switzerland.

Sleep, N. H. (1995), Ductile creep, compaction, and rate and state dependent friction within major fault zones, *J. Geophys. Res.*, *100*(B7), 13065-13080, doi:10.1029/94JB03340.

Tsutsumi, A., and T. Shimamoto (1997), High-velocity frictional properties of gabbro, *Geophys. Res. Lett.*, *24*(6), 699-702, doi:10.1029/97GL00503.

Tullis, T. E., and D. L. Goldsby (2003), Flash melting of crustal rocks at almost seismic slip rates, *Eos Trans. AGU*, *84*(46), Fall Meet. Suppl., Abstract S51B-05.

Zheng, G., and J. R. Rice (1998), Conditions under which velocity-weakening friction allows a self-healing versus a crack-like mode of rupture, *Bull. Seismol. Soc. Am.*, *88*, 1466-1483.

Department of Physics, University of California, Santa Barbara, CA, 93106-9530

Table 1. Parameters for dynamic rupture simulations. Shared model parameters are: grid spacing dl, number of spatial grid points nx, shear modulus μ, shear wave speed c_s, Poisson's ratio ν, Courant-Friedrichs-Lewy Ratio cfl $= c_s dt/dl$ (determines the time step dt), length of the fault permitted to rupture L_{fault}, size of the triggering patch L_{trigg}, initial shear load τ_{load}, and stress in the triggering patch τ_{trigg}. The frictional parameters are discussed with each model in the main text.

Dynamic Rupture Simulation Parameters	
Shared Parameters	SW Law
$dl = 0.01$ km	$d_c = 0.31$ m
$nx = 2048$	$\tau_p = 73.85$ MPa
$\mu = 32.03812032$ GPa	$\tau_d = 63.375$ MPa
$c_s = 3.464$ km/s	
$\nu = 0.25$	
cfl $= 0.3$	
$L_{\text{fault}} = 16$ km	
$L_{\text{trigg}} = 1.3$ km	
$\tau_{\text{load}} = 68$ MPa	
$\tau_{\text{trigg}} = 74$ MPa	
FV Law	DR Law
$\chi_s = 0.3407$	$L_{\text{DR}} = 21.5$ mm
$\sigma_d = 0.25$ MPa	$a = 0.0027$
$\chi_c = 0.1145$	$b = 0.0077$
$f_* = 222.3$	$f_0 = 0.7$
$V_* = 10^{-6}$ m/s	$V_0 = 10^{-6}$ m/s
$R_c = 5$ s^{-1}	$\sigma = 100$ MPa
$\alpha = 0.0005$ (MPa m)$^{-1}$	$V_1 = 10^{-6}$ m/s
$\chi_h = 0.0028$	
$\tau_0 = 44.12$ MPa	
$\chi(t = 0) = 0.0061$	$\theta(t = 0) = 21500$ s

Table 2. Parameters for DR and FV law dynamic ruptures with rapid weakening. Symbols for the shared model parameters are defined in Table 1, except for the characteristic rapid weakening velocity V_W.

Rapid Weakening Simulation Parameters	
Shared Parameters	
$dl = 0.004$ km	
$nx = 2048$	
$\mu = 32.03812032$ GPa	
$c_s = 3.464$ km/s	
$\nu = 0.25$	
cfl $= 0.3$	
$L_{\text{fault}} = 6$ km	
$L_{\text{trigg}} = 1.3$ km	
$\tau_{\text{load}} = 22$ MPa	
$\tau_{\text{trigg}} = 74$ MPa	
$V_W = 1$ m/s	
FV Law	DR Law
$\chi_s = 0.3407$	$L_{\text{DR}} = 50$ mm
$\sigma_d = 0.25$ MPa	$a = 0.0027$
$\chi_c = 0.1145$	$b = 0.017$
$f_* = 222.3$	$f_0 = 0.7$
$V_* = 10^{-6}$ m/s	$V_0 = 10^{-6}$ m/s
$R_c = 5$ s^{-1}	$\sigma = 100$ MPa
$\alpha = 0.0005$ (MPa m)$^{-1}$	$V_1 = 10^{-6}$ m/s
$\chi_h = 0.0028$ m	
$\tau_0 = 44.12$ MPa	
$\chi(t = 0) = 0.0061$	$\theta(t = 0) = 50000$ s

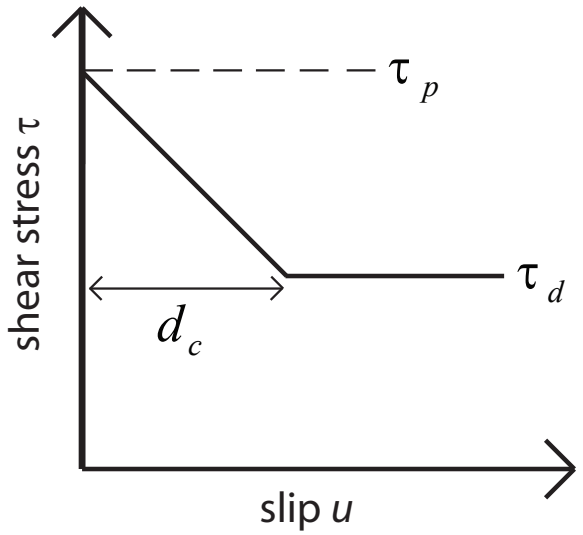

Figure 1. Prescribed shear stress evolution for the linear SW law. Slip initiates when the shear stress reaches the peak strength τ_p. Over a slip distance d_c, stress weakens linearly to a constant dynamic sliding friction τ_d. Because the sliding friction τ_d is constant, no dynamic recovery of strength occurs for the SW law.

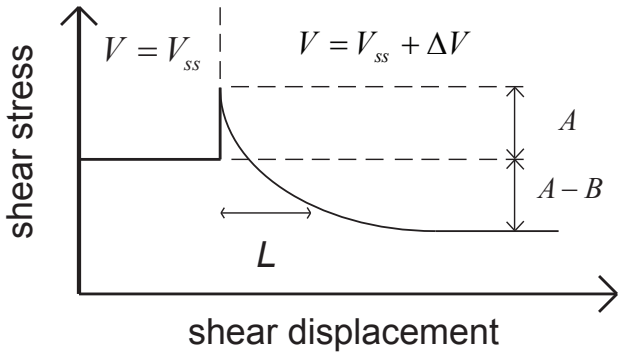

Figure 2. Shear stress versus slip for a velocity step experiment. The slip velocity is perturbed from steady sliding at V_{ss} to $V_{ss} + \Delta V$, and the transient response of the system is shown. The instantaneous increase in friction (A), the length scale for evolution (L), and the new steady-state ($A - B$) are shown in the plot.

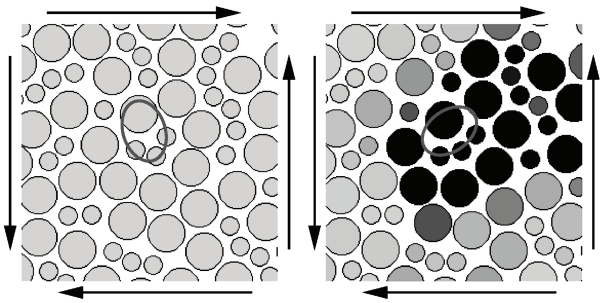

Figure 3. Schematic of an STZ undergoing transformation from one metastable orientation (left) to the other (right). The applied shear stress is denoted by the arrows. As the gouge deforms plastically, the ellipse drawn through the particles flips its orientation. Figure taken from *Falk and Langer* [1998].

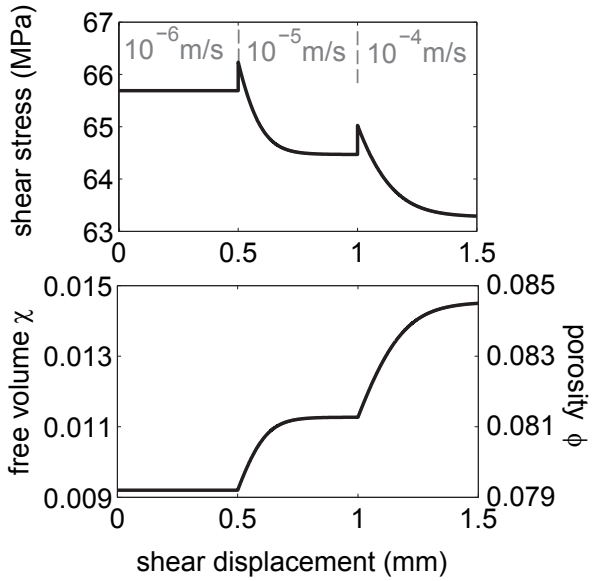

Figure 4. Dynamic evolution of the stress and free volume/porosity during two simulated velocity step experiments. The first velocity step from $V = 10^{-6}$ m/s to $V = 10^{-5}$ m/s occurs at 0.5 mm, and the second velocity step from $V = 10^{-5}$ m/s to $V = 10^{-4}$ m/s occurs at 1 mm. The transient changes in stress are the same for both velocity steps, confirming the logarithmic velocity dependence of the FV law. The length scale L_{FV} is larger for the second velocity step, which verifies that the length scale depends on the slip rate. The increased length scale at larger slip rates is easier to see in the lower plot, as the free volume is still evolving on the right edge of the plot but has stabilized within the same displacement during the first velocity step. The change in porosity is small compared to the total porosity, indicating that the change in the sheared layer thickness is small compared to the overall thickness. The porosity evolution uses $\phi_0 = 0.07$ to convert from free volume.

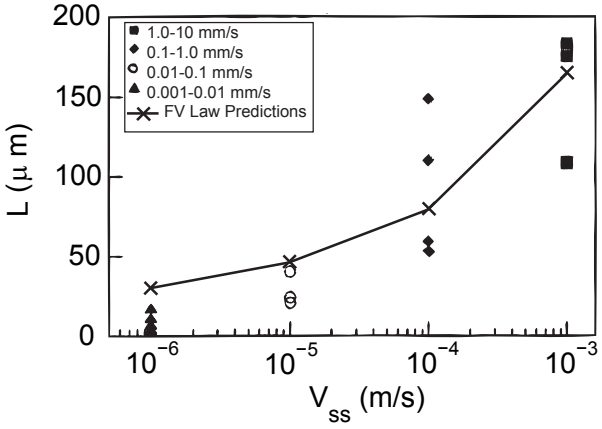

Figure 5. Experimental data for L [*Mair and Marone*, 1999] and the corresponding predictions of the FV law. The FV law predictions are given by Eq. (19) with the following parameters: $\chi_s = 0.3407$, $\sigma_d = 0.25$ MPa, $\chi_c = 0.1145$, $f_0 = 222.3$, $V_0 = 10^{-6}$ m/s, $R_c = 5$ s^{-1}, $\alpha = 0.3$ (MPa s)$^{-1}$, $\chi_h = 0.0028$, and $\tau_0 = 44.12$ MPa. The DR law predicts that L is independent of slip rate – the above plot is a horizontal line for DR friction. The FV law follows the observed trends in laboratory faults.

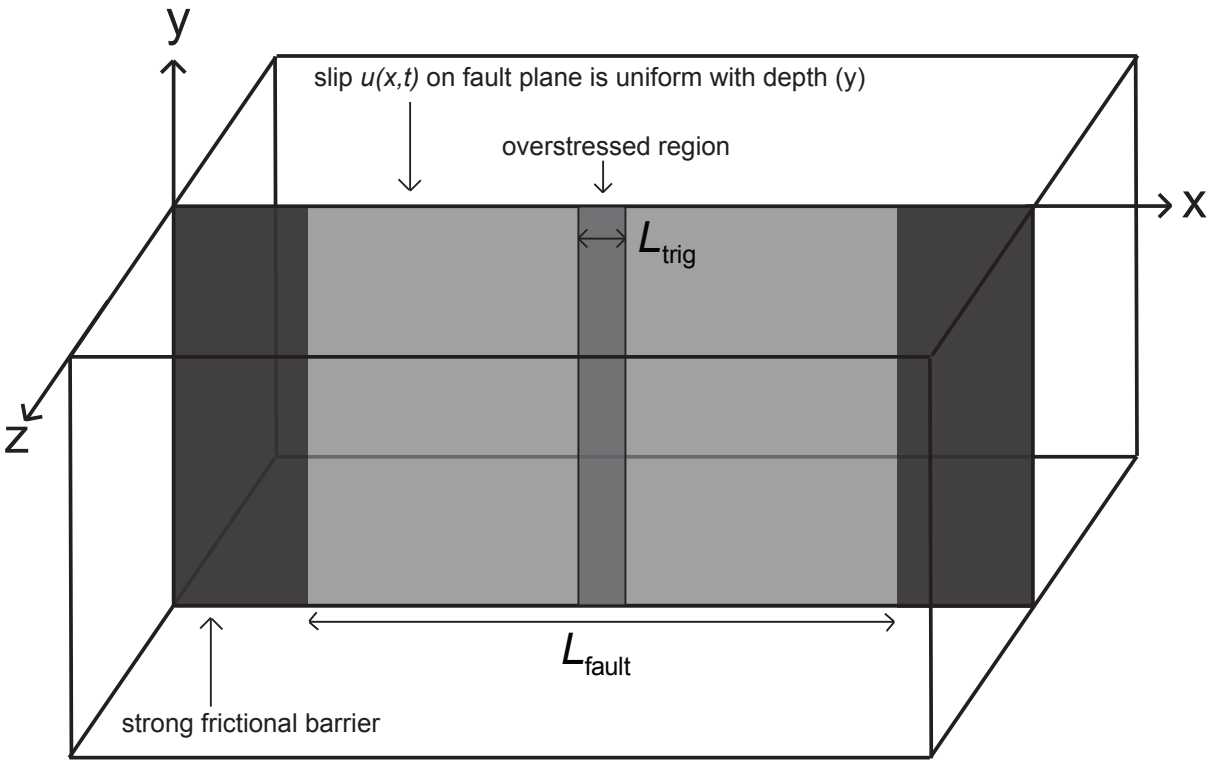

Figure 6. Schematic of the fault used in dynamic rupture calculations. Two identical homogeneous, isotropic, linear elastic half spaces are loaded far from the fault. Slip varies only in the x-direction, and boundary conditions are periodic. The symmetry in the y-direction requires that the slip and slip rate are scalars, either in the x-direction for in-plane loading or in the y-direction for anti-plane loading. The initial load is uniform except for an overstressed patch (medium shade of gray) which triggers rupture, and friction parameters are uniform except for strong barriers (darkest shade of gray) to prevent periodic replicas from affecting the solution.

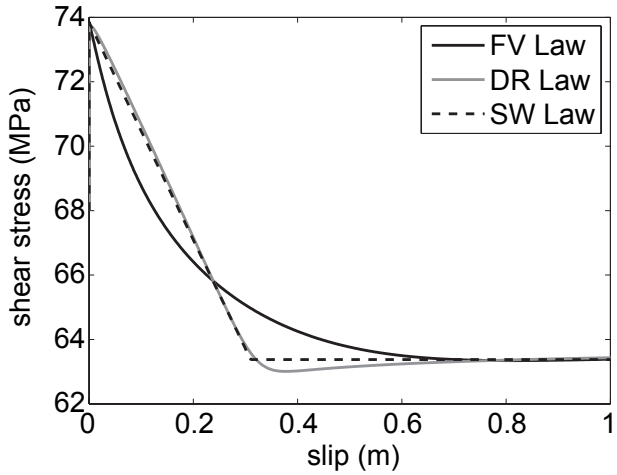

Figure 7. Plots of shear stress as a function of slip for an anti-plane rupture at a point 4 km away from the hypocenter for the linear SW, FV and DR laws. The SW law weakens linearly with slip by construction. The DR law also exhibits linear weakening with slip, and its close match to the SW law is due to intentional choice of parameters. The FV law weakens more rapidly with initial slip due to the small value of L_{FV} at low slip rates, while weakening is more gradual at larger slips when the fault slips more rapidly. The FV law requires more total slip to fully weaken to its minimum shear stress. The shear stress increases slightly for the FV and DR laws beyond the range of the plot as the time-dependent healing in each law results in some re-strengthening. Parameters were chosen for the laws to have equal areas under the slip weakening curve and thus have the same energy lost to frictional dissipation. Parameters are given in Table 1.

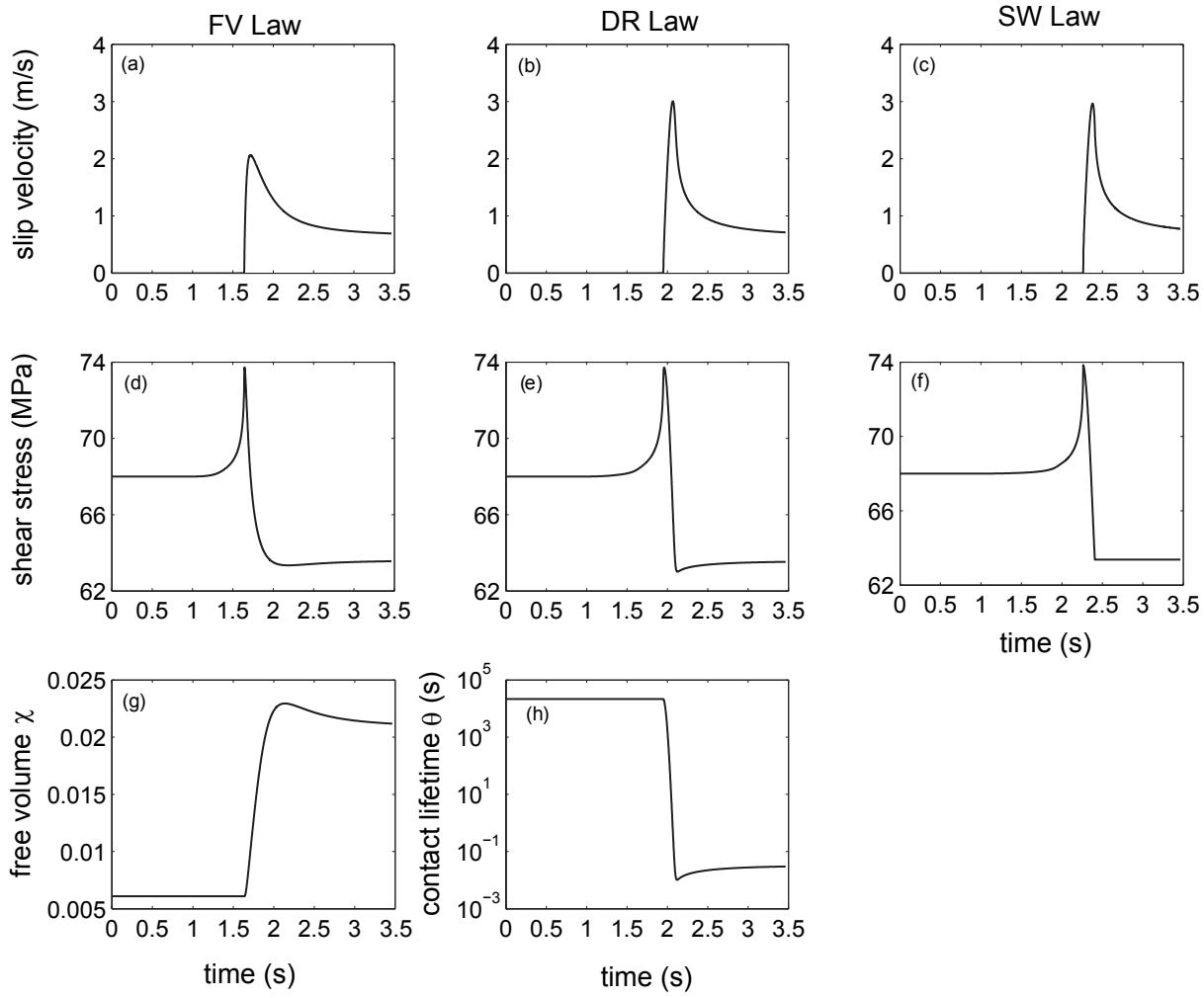

Figure 8. Fault dynamics during rupture at a point 4 km away from the hypocenter for the FV (a,d,g), DR (b,e,h), and SW (c,f) laws. As a function of time, (a)-(c) plot slip rate, (d)-(f) plot shear stress, and (g)-(h) plot the appropriate state variable for the FV or DR law. The velocity plots show all laws support expanding crack solutions. The FV law rupture arrives slightly earlier – the rupture reaches the limiting shear wave speed more rapidly due to the smaller nucleation length in the FV law. The peak slip velocity is also smaller for the FV law. The ruptures governed by the SW and DR laws have nearly identical time dependence of slip rate and shear stress. The DR law rupture arrives slightly earlier, but otherwise the laws produce matching ruptures. Shear stress increases at the crack tip to induce slip, and the minimum shear stress occurs at the extreme value of the respective state variable for the FV and DR laws. Parameters are given in Table 1.

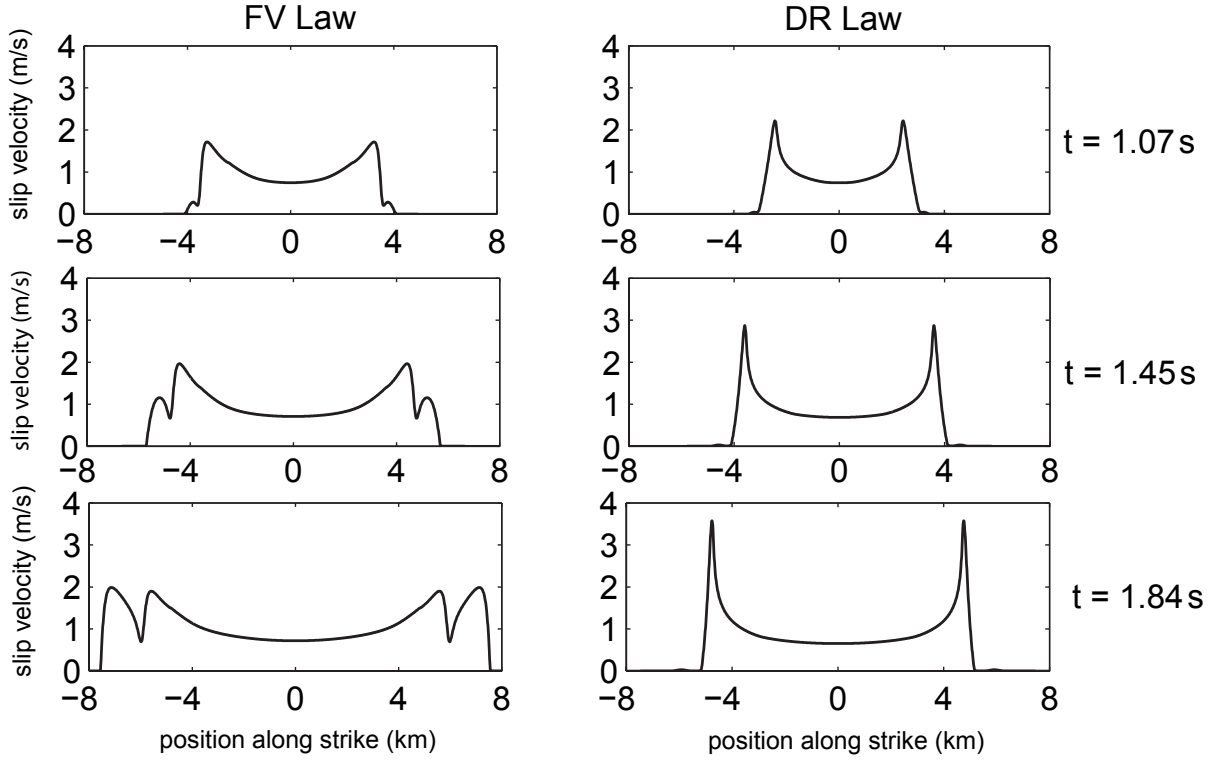

Figure 9. Snapshots of slip velocity along strike at three different times. Results are plotted for the FV law on the left and the DR law on the right. Initial conditions on the fault are identical, as is the amount of energy lost to frictional dissipation. The smaller nucleation size of the FV law allows the rupture to transition to supershear, while no supershear rupture occurs for the DR law. Parameters are the same as in Table 1 except $\tau_{\text{load}} = 69$ MPa, $R_c = 5.7$ s^{-1}, $\alpha = 0.00057$ (MPa m)$^{-1}$, $l = 18.45$ mm, and $\theta(t = 0) = 18450$ s.

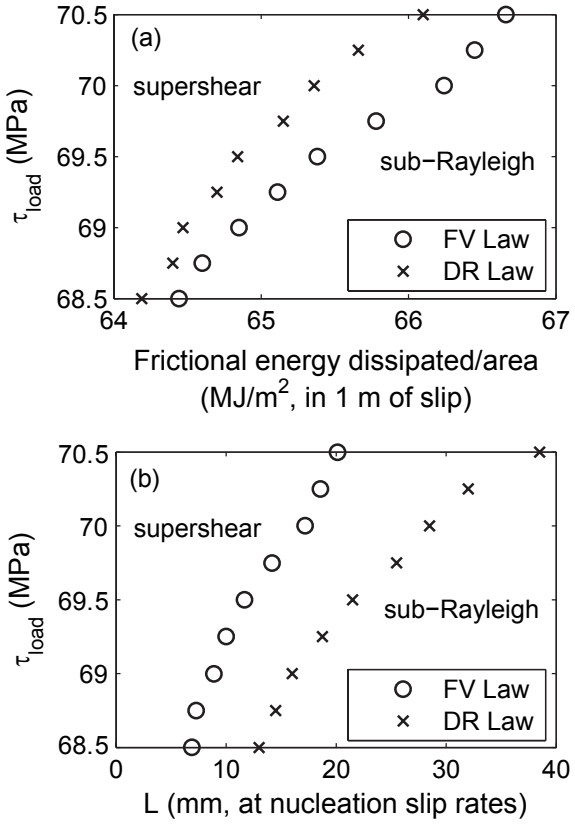

Figure 10. Rupture type diagrams for in-plane ruptures with the FV and DR laws as a function of the initial shear load and (a) energy per unit area dissipated by friction during the first meter of slip at a point 4 km from the hypocenter, (b) L at nucleation slip rates. Each individual point on the plot is the largest energy per area or L at which unstable supershear rupture is observed to develop on the bounded fault. Above and to the left of these points, supershear ruptures will occur, and below and to the right crack growth is confined to sub-Rayleigh speeds. For equal dissipated frictional energy (a), the FV law curve is further to the right and a region exists between the curves where the FV law transitions to supershear and the DR law does not (Fig. 9 illustrates a specific example in this region). In (b), the DR law curve sits to the right, and DR law can rupture faster than the shear wave speed while the FV law does not for identical initial shear loads.

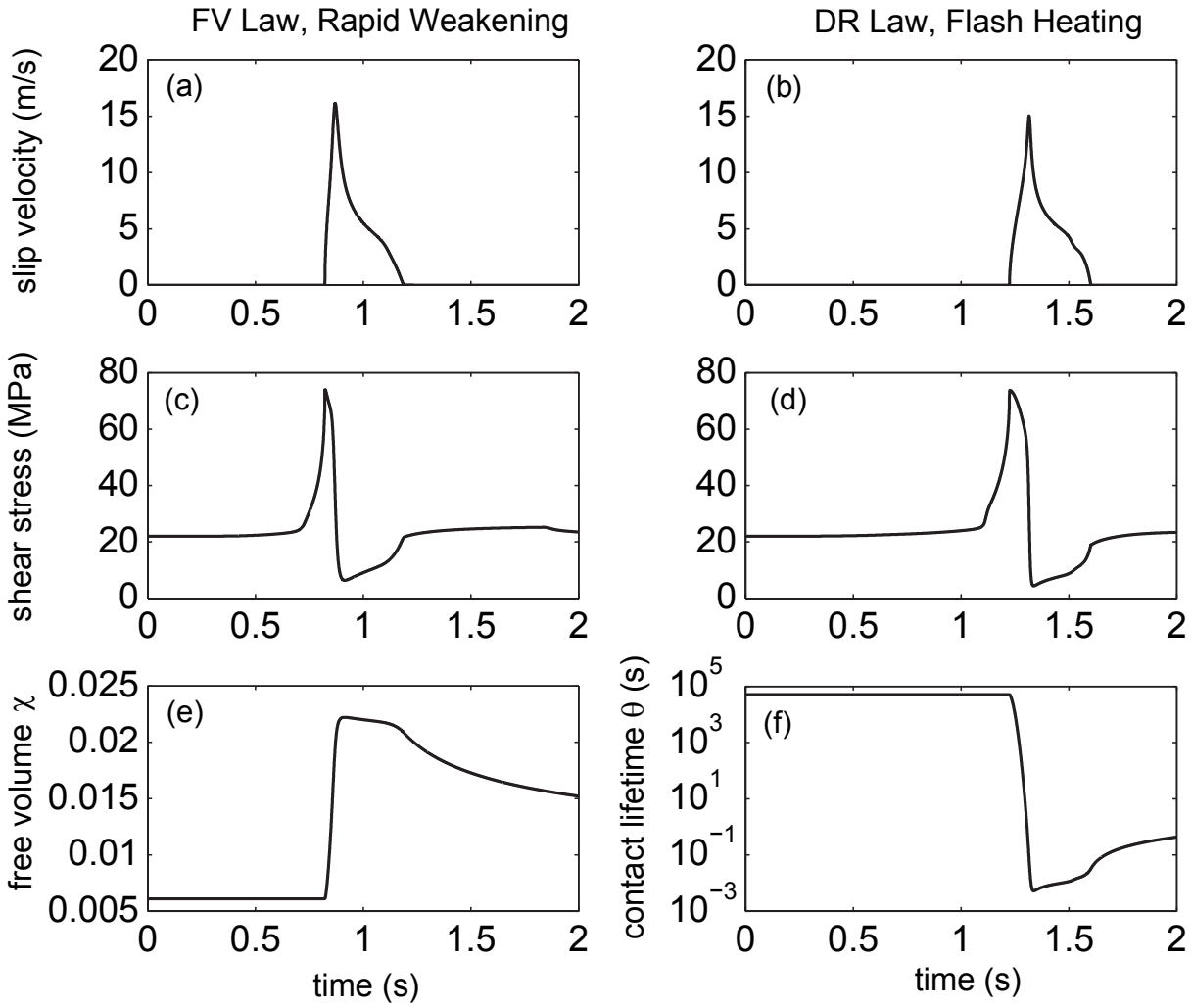

Figure 11. Fault dynamics for rapid weakening friction models. (a-d) Both laws rupture as self-healing pulses with low initial loading stresses. The slip rates are larger than with the laws without rapid weakening. (e) Because the evolution equation for the free volume depends on the stress (Eq. (15)), rapid weakening alters the free volume dynamics. After a rapid period of dilation, free volume varies little over a wide range of slip velocities before the fault heals and compaction begins. (f) State variable evolution for the DR law with flash heating. The contact lifetime drops rapidly with the arrival of the rupture, and increases with time once the fault heals to regain frictional strength. Parameters for these anti-plane simulations are given in Table 2.

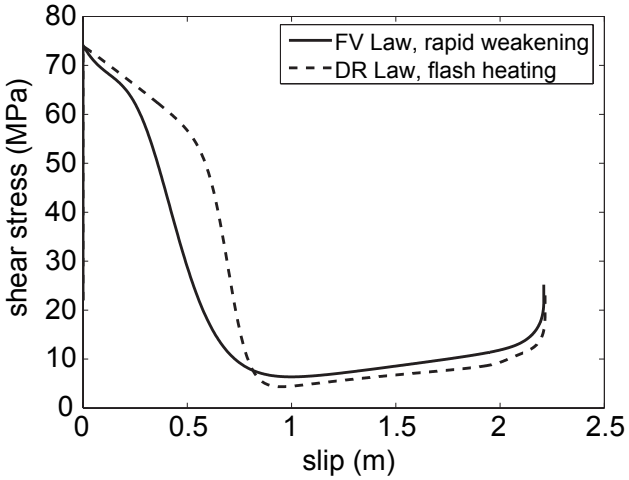

Figure 12. Shear stress as a function of slip for antiplane dynamic ruptures with the rapid weakening friction laws. Parameters were selected for each pulse to yield the same net slip (the DR law dissipates more energy in frictional sliding). As with the laws without rapid weakening, the FV law weakens more rapidly with initial slip, and more gradually during rapid slip. Matching slip between the laws requires a significantly larger value of L_{DR} than in ruptures without rapid weakening. As a consequence, the DR b parameter must be increased to give the two laws comparable nucleation lengths. Without this change, the flash heating model will not rupture with identical initial shear loads. Parameters for these simulations are given in Table 2.

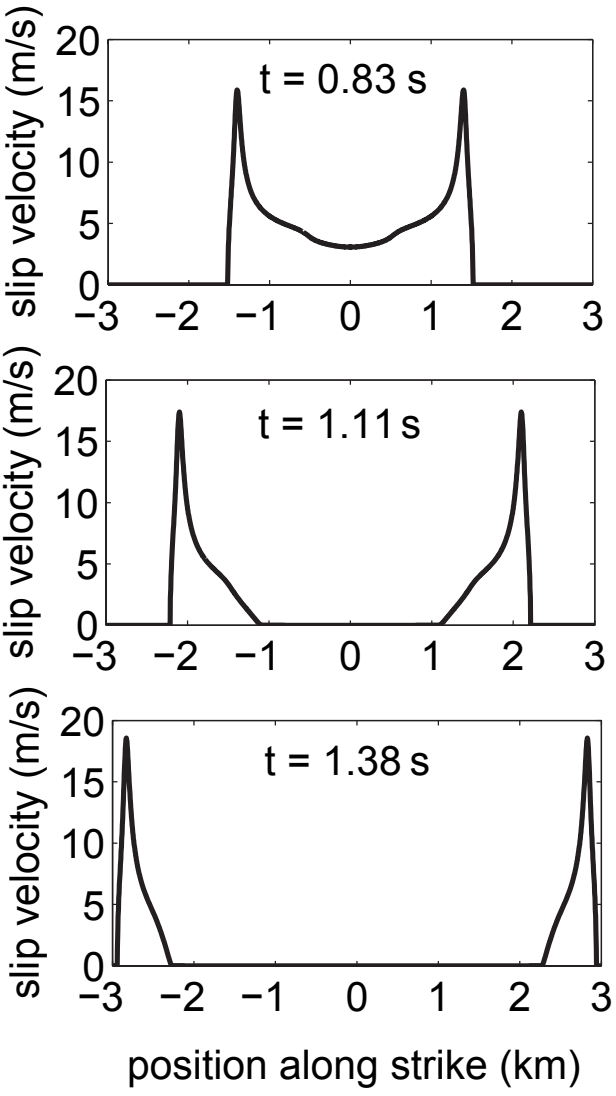

Figure 13. Snapshots of slip velocity as a function of position for anti-plane rupture with the rapid weakening FV law. The slip rate is shown at three different times, illustrating how the rupture evolves in both space and time. In the top plot, slip is propagating as an expanding crack. As time progresses in the subsequent plots, slip ceases in the center of the fault and the rupture continues as an expanding pulse. The slip velocity evolves in a similar manner for the DR law with flash heating, though the rupture is slower to advance out to the ends of the fault. Parameters for this simulation is given in Table 2.

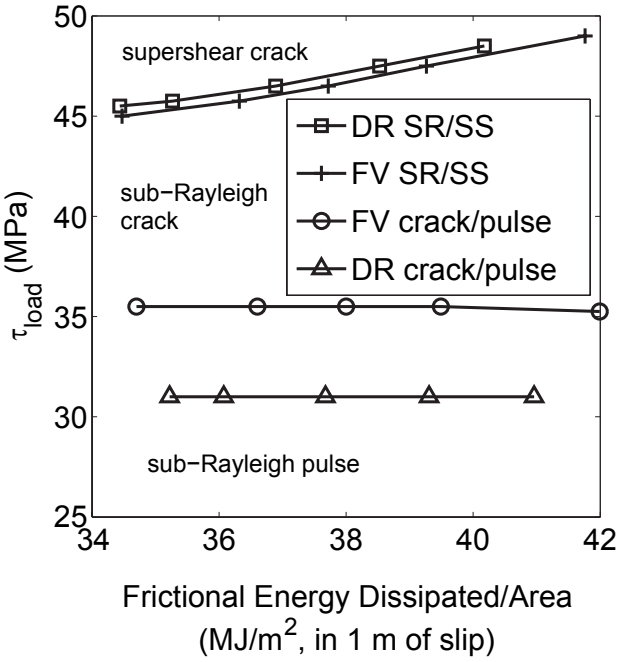

Figure 14. Rupture type diagram for in-plane ruptures with rapid weakening. Points on the plot indicate the smallest initial shear stress for which supershear rupture or sub-Rayleigh crack-like rupture is observed on the fault for a given amount of energy dissipated to friction. Above the sub-Rayleigh/supershear (SR/SS) transition, the rupture is a supershear crack. Below the crack/pulse transition line, the rupture is a sub-Rayleigh pulse. Between the two lines, the rupture is a sub-Rayleigh crack. The crack/pulse transition is independent of the frictional energy dissipated for a given law, consistent with the anti-plane study of *Zheng and Rice* [1998]. However, we note that the DR law requires lower initial loads for pulse-like rupture than the FV law despite identical steady-state velocity weakening. The sub-Rayleigh/supershear transition depends on the specifics of frictional dissipation, with only a slight difference between the DR and FV laws. Parameters are the same as in Table 2 except for the initial loading stress τ_{load} and the friction parameters α and R_c for the FV law or l and $\theta(t = 0)$ for the DR law, which are varied in the simulations.